University of Stavanger

Faculty of Science and Technology

MASTER'S THESIS

Study program/Specialization: **Petroleum Technology/Drilling and Well Technology**	**Spring semester, 2019** **Open** / ~~Confidential~~
Author: **Parisa Ghaedi**	**Digital submission** ~~(signature of author)~~
Supervisor(s): **Mahmoud Khalifeh (UiS), Arild Saasen (UiS), Tor Henry Omland (Bitrunner)**	
Title of master's thesis: **A Study of the Effect of Pressure and Temperature on the Mechanical Friction of Four Different Fluids Using a Specially Designed Setup**	
Credits: **30 ECTS**	
Key words: **Friction** **Mechanical friction** **Excessive torque and drag** **Drilling fluids** **Lubricants** **Pressure** **Temperature**	Number of pages: **78** +supplemental material/other: **0** Stavanger, **13th June 2019**

A Study of the Effect of Pressure and Temperature on the Mechanical Friction of Four Different Fluids Using a Specially Designed Setup

By Parisa Ghaedi

ACKNOWLEDGEMENTS

Parisa Ghaedi

Stavanger, 2019

ABSTRACT

The mechanical friction caused by the contact between the rotating drillstring and the borehole or casing can lead to significant challenges such as excessive torque and drag, limitation in running speed of drillstring and liners, pipe buckling or tubular twist-off and in severe cases complete loss of the well. Thereby, to optimize different operations with respect to such challenges, proper understanding and estimation of the mechanical friction as well as the factors which affect it, is important. In this project, a general review has been performed on the concept of mechanical friction in a wellbore. Also, the challenges caused by mechanical friction particularly during drilling and intervention operations have been discussed. In addition, different setup or instruments used by several researchers to study the effect of different parameters on the mechanical friction have been reviewed and their limitations have been pointed out.

This thesis project is essentially an experimental study which deals with investigating the effect of pressure, temperature and their combined effect on the friction coefficient of deionized water, mineral oil, oil-based and water-based mud. For this purpose, an experimental setup has been designed at the University of Stavanger which works in combination with an automated high-pressure, high-temperature consistometer from OFI Testing Equipment. Using the designed setup, several experiments were performed on the mentioned fluids at constant temperatures of 25 and 50°C, while the pressure increased from 69 bar to 345 bar at both temperatures.

In summary, it was found that, with the exclusion of the deionized water at 50°C and the oil-based mud at 25°C, pressure increase did not have a significant effect on the friction coefficient of the other fluids at the defined temperatures. Also, the change in temperature from 25 to 50°C led to a decrease in friction coefficient values of all the fluids except the deionized water. In addition, it was observed that at both temperatures, the mineral oil had the lowest values of friction coefficient compared to the other fluids while deionized water had the highest values.

TABLE OF CONTENTS

LIST OF FIGURES

LIST OF TABLES

ABBREVIATIONS

API	American Petroleum Institute
BHA	Bottom Hole Assembly
CT	Coiled Tubing
DLS	Dog Leg Severity
ERW	Extended Reach Well
HPHT	High-Pressure High-Temperature
LEM	Lubricity Evaluation Monitor
LPM	Liters Per Minute
NADF	Non-Aqueous Based Drilling Fluid
OBM	Oil-Based Mud
PPFRT	Pressure Pulse Friction Reduction Tool
RPM	Revolutions Per Minute
ROP	Rate of Penetration
UCS	Uniaxial Compressive Strength Tester
WBM	Water-Based Mud
WOB	Weight on Bit

1 INTRODUCTION

Mechanical friction is one of the significant issues in different operational phases of a well as it can lead to severe challenges as well as increased rig time and cost. To optimize different operations with respect to mechanical friction, it is necessary to obtain a proper understanding of the mechanical friction, the different parameters which have an impact on it and the methods used to mitigate it.

Therefore, in this section, a general review has been performed on the concept of friction and mechanical friction as well as the different factors which affect mechanical friction in a wellbore. Also, the challenges caused by mechanical friction particularly in drilling and intervention operations have been discussed. Further, some of the methods used in the industry to mitigate such challenges have been argued. In addition, several setup or instruments used by different researchers to study the different factors which affect mechanical friction have been reviewed and their limitations have been mentioned.

1.1 General concept of friction

Basically, friction can be defined as a force which always acts opposite to the direction of motion of two surfaces which are moving relative to each other. Friction belongs to the science of tribology which itself comes from the Greek word tribos that means rubbing. Rubbing is in fact the action which occurs when two objects are in motion relative to each other (Bhushan, 2013; Dowson, 1998; Persson, 2000). Leonardo Da Vinci (1452-1519) was an engineer/artist of the Renaissance period who figured out the dominating rules of the sliding motion of a rectangular object over a flat surface. He also presented the theory of the coefficient of friction for the first time and defined it as the ratio of the friction force to the normal force. Later, in 1699, Guillaume Amonton, who was a French physicist, came up with the two laws of friction based on his studies of the sliding motion of two dry, flat surfaces. The first law states that the friction force has direct proportionality to the applied load. The second law expresses the fact that the friction force is not dependent on the area of contact between the two objects in motion (Bhushan, 2013; Bowden and Tabor, 1964). So, it does not matter how large the contact area between the two objects is. In fact, what matters are the interlocking asperities inside each of the objects in contact which should overcome the friction force in order for the two objects to start moving relative to each other. In 1785, Charles-Augustin Coulomb, who was a French

physicist, approved Amonton's work and came up with the third law of friction. The third law states that the kinetic friction does not depend on the sliding velocity of the two objects in motion (Bhushan, 2013; Bowden and Tabor, 1964). Therefore, the friction force will always exist independently of the velocity of the two moving objects in contact.

1.1.1 Mechanical friction factor or the coefficient of friction

Mechanical friction factor is a term used to refer to Coulomb friction or the coefficient of friction. Friction coefficient is a scalar value which is dimensionless and is defined as the ratio of the friction force over the normal force applied to the objects in contact. The friction coefficient can thus be calculated using Eq.1.

$$\mu_i = \frac{F_f}{N} \tag{1}$$

where,

μ_i stands for either the static or kinetic coefficient of friction. F_f stands for the friction force and N stands for the normal force applied to the objects in contact (Samuel, 2010).

1.1.2 Different types of friction force

Static friction force occurs when two objects are in contact but none of which are moving. The static friction force thus prevents the motion of the two objects in contact. The kinetic friction force happens as soon as one of the objects in contact starts to move relative to the other and is a force acting against the direction of motion. Also, the kinetic friction force is less than static friction force which prevents the two objects in contact from moving. Fig. 1.1 illustrates a plot of static and kinetic friction coefficients. Furthermore, the static coefficient of friction is defined as the ratio of the friction force necessary to start motion to the normal force applied to the two contact surfaces. The kinetic coefficient of friction on the other hand is defined as the ratio of the friction force necessary to keep the two contact surfaces in motion to the normal force applied to the contact surfaces (Redburn et al., 2013; Samuel, 2010).
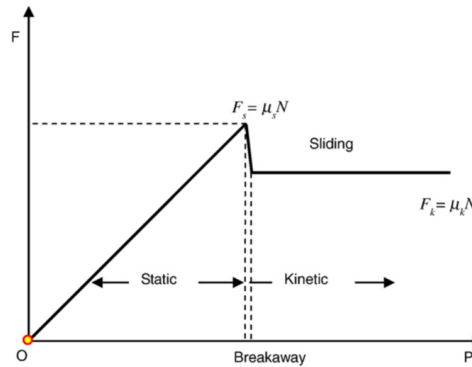
Fig. 1.1 Force of friction as a function of pulling force (after Samuel (2010)).

Other types of kinetic friction force include rolling and rolling/sliding friction force. Rolling friction force happens when one of the objects in contact starts rolling relative to the other one. Rolling/sliding friction force on the other hand, happens in conditions when the objects in contact slide and roll simultaneously relative to each other. The friction coefficients associated with the rolling or rolling/sliding friction forces are usually measured through empirical tests and cannot be calculated (Samuel, 2010).

1.2 Mechanical friction in a wellbore

Mechanical friction can be defined as a resistive force to the motion of two solid surfaces which are moving relative to each other (Rabinowicz, 1995). In a wellbore, mechanical friction must be mitigated in various circumstances as it is a limiting factor which can lead to increased rig time and cost. Different types of mechanical friction constantly occur in different sections of a wellbore. For instance, the friction caused by the contact between drill pipe and tubing or casing is an example of steel on steel mechanical friction. Also, the friction caused by the contact between drillstring or drill bit and the formation is an example of steel on rock mechanical friction.

1.2.1 Different factors that affect mechanical friction

Generally, mechanical friction can be affected by several different factors such as drilling fluid type and composition, wellbore trajectory, geometry of the pipe, wellbore conditions, etc. Among the wellbore conditions that affect mechanical friction, one can refer to keyseats, ledges

and washouts. Also, the mechanical friction caused by the contact between the drillstring and the formation can vary by several downhole parameters. These parameters may include pressure, temperature, geometries and properties of contact surfaces, applied loads, properties of drilling fluid and filter cake, etc. (Maidla and Wojtanowicz, 1990). In certain circumstances, some of the mentioned factors and parameters can increase the mechanical friction while others tend to reduce it. Therefore, a proper evaluation of the various factors which may have an impact on mechanical friction is essential during the different operational phases of a well.

1.2.2 Challenges caused by mechanical friction

Mechanical friction is considered a major challenge specifically in extended reach wells (ERW), highly inclined and horizontal wells. Nowadays, with the ERWs reaching the length of 12 345 m, mechanical friction may cause serious issues such as high surface torque and inadequate weight transfer to the bit (Walker, 2012). In ERWs which also include highly deviated wells, the drillstring usually tends to lie on the low side of the borehole wall compared to wells with lower degree of deviation. This happens due to the effect of gravity. Generally, as the length of the drillstring and the degree of vertical deviation increase, the friction force associated with the contact between drillstring and the borehole also increases (Taghipour et al., 2014; Taghipour et al., 2015; Ytrehus et al., 2017). The generated friction force practically causes a drag force which can be either a positive force for instance during pulling the drillstring out of the hole, or a negative force for instance during running and sliding the drillstring into the borehole. Also, during the rotation of the drillstring, the same friction force decreases the surface torque transferred to the bit (Mitchell and Samuel, 2007).

During the lifetime of a well, mechanical friction can also lead to serious challenges in different operations (Foxenberg et al., 2008; Livescu et al., 2014; Taghipour et al., 2014). For instance, it can limit and reduce the tripping or running speed of drill strings and liners. Exceeding the limits of running speed can lead to stuck pipes or breakouts and reduced running speed of casings and liners increases the nonproductive time during drilling and completion operations (Ytrehus et al., 2016). Also, the mechanical friction caused by the contact between the rotating drillstring and the borehole or casing can lead to significant issues such as excessive torque and drag which by itself can result in other severe problems. Among these problems one can list: limitation in achieving the target depth, overpull while tripping out, stuck pipe, pipe buckling or tubular twist off and in severe cases complete loss of the well (Aarrestad, 1994; Dzialowski et al., 1993; Sönmez et al., 2013; Taghipour et al., 2014; Taghipour et al., 2015;

Ytrehus et al., 2017). In addition, excessive torque and drag can cause limitation in reaching the desired lateral length while running coiled tubing (CT) during intervention operations particularly in ERWs (Livescu et al., 2014). In the following section, different factors that result in excessive torque and drag are discussed.

1.2.2.1 Different factors that result in excessive torque and drag

Basically, torque can be defined as the necessary moment which is essential for pipe rotation and drag is a force which is required for running the pipe into the hole or pulling the pipe out of the hole (Mirhajmohammadabadi et al., 2010). There are several circumstances which usually result in excessive torque and drag in a wellbore. These may include sliding wellbore friction, cuttings bed buildup as a result of poor hole cleaning, differential sticking, tight hole or sloughing hole conditions, keyseats, etc. Apart from sliding friction, all the other mentioned circumstances which cause excessive torque and drag, are related to wellbore conditions. On the other hand, in wells with suitable wellbore conditions, the main reason which leads to excessive torque and drag is the sliding friction (Johancsik et al., 1984; Mirhajmohammadabadi et al., 2010; Sheppard et al., 1987). Well path geometry is also another important factor which may contribute to excessive torque and drag. To lower the torque and drag, drilling more straight and smooth wells is thus essential. Fig. 1.2 shows the torque and drag forces in different sections of a wellbore. As it can be observed from Fig. 1.2, the distribution of the side forces in a wellbore depends on the variations of dogleg severity (DLS) in buildup, drop-off and bend sections. For instance, in sharp bends with smaller radius, the side forces are more focused and pointed towards an individual section of the wellbore. Contrarily, in large radius bends, the side forces are distributed more evenly in the wellbore. The even distribution of side forces in the wellbore can considerably decrease the torque and drag particularly at the top sections of the well where the highest tensile forces exist. Thereby, proper well path design during the planning phase of a well is one of the most efficient ways to decrease the forces associated with torque and drag and mechanical friction. (McCormick et al., 2011; Ytrehus et al., 2017).
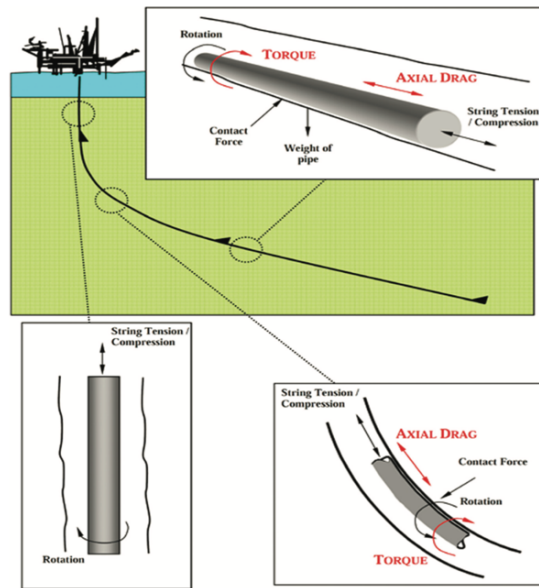
Fig. 1.2 Drillstrings' torque and drag forces in different sections of a wellbore (after Ytrehus et al. (2017)).

1.3 Mechanical friction challenges during different operations

To optimize the operations, estimation and understanding of the anticipated friction forces are of great significance (Ytrehus et al., 2016). It is also important to identify the different challenges that can be caused by mechanical friction during the different operations. In the following sections, examples of the various issues caused by mechanical friction during drilling and intervention operations have been discussed.

1.3.1 Mechanical friction challenges during drilling operations

Generally, friction plays a significant role in drilling operations. It is consequently of great importance to take the friction into consideration during tripping the drillstring in and out of the wellbore or rotating it on and off bottom. In addition, the friction force should be considered for calculation of torque and drag in solid mechanics as well as surge and swab in hydraulics. Friction force is also required for evaluating the hookload during cementing operations. It is quite complicated to simulate the drilling operations with friction force due to several different uncertainties. Some of these uncertainties include drilling fluid type, composition and lubricity, wellbore curvature, dogleg or keyseat, borehole torsion, cuttings bed, wellbore tortuosity, borehole diameter, surface roughness, etc. (Samuel, 2010).

ERWs, horizontal and deviated wells are considered the most effective and yet most complicated well technologies for the exploitation of oil and gas reserves. One of the main

challenges which occurs during sliding drilling operations in such wells is that the drillstring does not rotate. This can lead to a large enhancement in mechanical friction between the drillstring and the wellbore wall which can result in insufficient transfer of weight to the drill bit. This issue will not only decrease the rate of penetration (ROP) but also restrain the maximum desirable wellbore extension (Wang et al., 2018).

During drilling deviated wells, the mechanical friction between the drill string and the borehole can cause excessive torque and drag which can also contribute to poor weight transfer to the bottomhole assembly (BHA) and the drill bit. Consequently, the following issues may also occur:

- Restricted and inadequate monitoring and controlling of the tool-face. This can increase the wellbore tortuosity and lead to severe issues during running the casing, liner and completion strings.

- Stick-slip is one of the most typical issues during the drilling operations. This is usually the result of torsional drag and can cause the drillpipe to twist and then untwist at high velocity. As a consequence, severe damages may happen to the components of the BHA.

- Poor weight transfer to the drill bit can restrain the lateral or horizontal length that is desired to be drilled. This usually occurs when the drag force is equal to the weight that can be accumulated on the drill pipe. Insufficient weight on bit (WOB) can thus restrict the access to the reservoir and prevent possible production from the well. This can be associated with high cost and time for the operator.

- Reduced ROP will also lead to high cost and nonproductive time during the drilling operations (Gee et al., 2015).

1.3.2 Mechanical friction challenges during intervention operations

Mechanical friction is considered a significant challenge also during intervention operations in long laterals as it can prevent reaching the desirable target. Nowadays, more than 30 to 40% of the ERWs which need to be intervened are not reachable by CT (Livescu et al., 2014). Also, to perform a successful CT operation in ERWs, it is important that the CT is capable of transferring sufficient WOB through the entire length of the well. However, CT's ability to achieve the desirable intervention target is restricted, due to the mechanical friction between the CT and the wellbore. As a matter of fact, in the North Sea and North America, CT with outer diameter of 2 and 2 3/8-in is used to be run in laterals as long as 12000 and 25000 ft (i.e.

about 3658 and 7620 m), respectively. With the CT- friction reduction technologies available today, such long laterals may not be intervened and serviced through their whole length. Therefore, to be able to reach the desired lateral length and mitigate mechanical friction during intervention operations, several tools and methods have been used and applied. For instance, to access the unreachable lateral length, increasing the CT's diameter could be a theoretical option. However, it is not practical as it causes issues with respect to onshore transportation and logistics and also restrictions in offshore deck loading or crane lifting. The use of CT tractor tools and fluid hammers may also be considered as other options which provide acceptable operational ranges. However, they may also lead to major restrictions and complicate the operations by enhancing the circulating pressures. In comparison with the mentioned options, the use of lubricants in parallel with other systems is considered one of the simplest and most performed methods to enhance CT reach and reduce mechanical friction (Livescu and Craig, 2017; Livescu et al., 2014). This is mainly due to lubricants' large availability and approximately low cost. In addition, lubricants provide quick laboratory testing with the current rotational friction testers which exist in the market (Livescu and Craig, 2017).

1.3.2.1 CT coefficient of friction

Craig (2003) performed an analysis of the predicted versus recorded weights' data of 33 wells operated by Statoil in the Norwegian sector of the North Sea. During this analysis, he came up with the idea of using only one friction coefficient for the entire CT's length. Based on the results from the analysis of 33 wells, he found out that one single friction coefficient with the constant value of 0.24 could be applied in all the analyzed wells. He also mentioned that the resulting friction coefficient value does not depend on the rates of production, the complexity of wellbore deviation and the sliding direction of the CT during running into the hole or pulling out of the hole. Craig's concept of constant friction coefficient has been used between the CT and wellbore ever since in the pre-planning phase of CT operations, especially in the wells with fluids such as produced water, sea water and fresh water. The CT's friction coefficient may change due to variabilities in contact surface roughness and temperature as well as the existence of scale and debris. However, an average value of the individual friction coefficient could be used through the total length of the CT. The constant friction coefficient value of 0.24 has thus been applied in the field specifically for 2-in CT operations in 5 1/2-in laterals with the length range of 5000 to 6000 ft (i.e. about 1524 to 1829 m). For longer laterals on the other hand, it is not possible to use this value. This is because the friction force which

corresponds to this value is too large considering that the CT can be cable of transferring an approximate WOB of 500 lbf (i.e. about 2224 N) (Craig, 2003; Livescu and Craig, 2017). Fig. 1.3 illustrates an estimation of the effect of friction coefficient on the possible CT's lateral reach in different circumstances with the application of several lubricants and a fluid hammer tool.
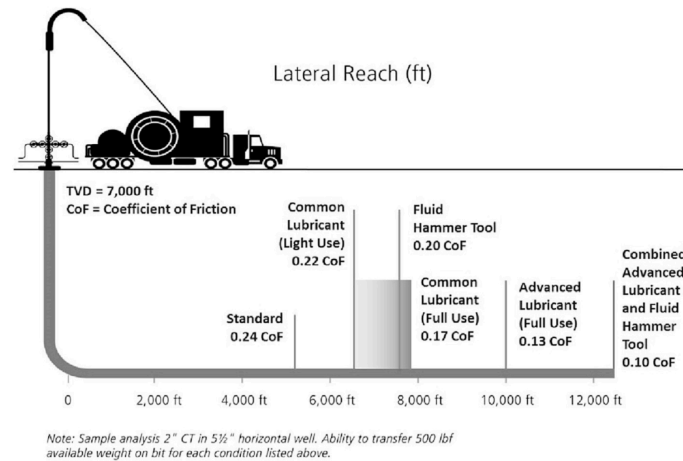
Fig. 1.3 An estimation of the effect of friction coefficient on CT's possible lateral reach with the application of several lubricants and a fluid hammer tool (after Livescu and Craig (2017)).

1.4 Solutions used to reduce mechanical friction

Conventionally, various methods have been used to decrease the mechanical friction between the drillstring and the borehole. Among these methods, one can list: increasing the lubricity of the drilling fluids, optimization of wellbore path and the drillstring's configuration, the use of drillstring with lighter weight, implementation of friction rollers and protection joints which are not rotating in short sections and the use of other types of friction reduction tools downhole (Wang et al., 2018). In the following section two of these methods are explained, namely, the application of friction reduction tools and the drilling fluid lubricants.

1.4.1 Friction reduction tools

Drilling of wells with complicated structures such as ERWs, deviated and horizontal wells, typically requires the application of rotary steerable systems. However, mechanical friction can cause severe issues along the length of the drillstring while drilling with steerable mud motors. This is due to the fact that such motors mostly perform sliding-drilling rather than rotating the drill pipe during directional drilling of a well. The application of friction reduction tools has been thus considered a beneficial solution to negative impacts of mechanical friction while

drilling with mud motors. This has been applied in horizontal wells in several fields in North America and has shown considerable reduction in torque and drag as well as mechanical friction (Gee et al., 2015). Generally, friction reduction tools are downhole tools which are implemented on the drillstring to decrease rotational friction as well as pipe and casing wear (Samuel, 2007). On the other hand, when it comes to drilling ERWs, lubricants are more preferable options for reducing the friction since extra tools are usually avoided in the borehole while drilling ERWs. Also, friction reduction tools are quite expensive compared to lubricants. Nonetheless, they have proven to reduce the torque and drag to a greater extent compared to lubricants (McCormick et al., 2011). Among the friction reduction tools, one can list: pressure pulse friction reduction tools (PPFRT), swivels and sub-based rollers.

1.4.1.1 Pressure pulse friction reduction tool (PPFRT)

PPFRT is a kind of friction reduction tool which creates vibration in the drillstring in order to mitigate and stop static friction. It causes axial motion in the drillstring through its own oscillation. The tool consists of a power section, a pulsing system and a bearing system. The fluid is injected into the drillstring through the power section while a rotor starts rotating inside a stator and forms a flow path which makes it possible for the pulsing system to create a sequence of pressure pulses. Consequently, the pressure pulses lead to drillstring's axial motion. The rotation of the drillstring as well as its axial vibration can decrease and eventually stop the static friction between the drillstring and the formation. The PPFRTs have shown considerable improvements in decreasing friction, transferring sufficient WOB to the drill bit and increasing ROP. Also, they are quite efficient when it comes to anti-stalling for motors and rotary steerable systems. Furthermore, they are particularly favorable in circumstances such as sliding drilling when the drillstring does not rotate (McCormick et al., 2011).

1.4.1.2 Swivel

Swivels are also another kind of friction reduction tools which are commonly employed in highly inclined wells for the purpose of running liners or completion strings. The swivel makes the independent rotation of the pipe above the screen or liner possible during running into the hole. The free rotation of the upper mandrel enables the swivel to change its condition from static to dynamic and consequently, decrease the forces of torque and drag. This will eventually lead to more downhole weight transfer. To operate the swivel, differential pressure is used

which locks the two mandrels in the tool together and makes the transmission of torque along the tool possible. Moreover, the drag caused by running strings can be considerably decreased by the swivel (McCormick et al., 2011).

1.4.1.3 Sub-based roller tools

The roller tools which are sub-based include a mandrel which rotates in a casting which is non-rotating. By lifting the string's tool joints off the borehole wall, the internal contact surfaces with lower friction can decrease the torque and drag particularly in wellbore sections where the normal force is higher. Also, in comparison with the tool joints, the roller tools have smaller contact surface areas against the borehole wall. Consequently, the roller tools will lower the possibility of differential sticking when they are employed in the open hole. These tools are most beneficial when located in wellbore sections with the highest torque and drag such as build section. In addition, they can be located both in cased and open hole (McCormick et al., 2011).

1.4.2 Drilling fluids' functionality and lubricity effect

Drilling fluids play a significant role in drilling operations. Some of the main functions of the drilling fluids include lubricating and cooling the drillstring and the drill bit, sustaining the stability of the borehole by keeping the hole size in-gauge, transporting the drill cuttings to the surface and avoiding the formation fluids to enter into the annulus (Bourgoyne Jr et al., 1986; Holder, 1982; Skalle, 2011).

Reducing the mechanical friction between the drillstring and the borehole or casing is also one of the most important associated functions of the drilling fluids (Caenn et al., 2016). Different properties of the drilling fluids can affect the mechanical friction and consequently, the torque and drag in a wellbore. Among these properties, one can mention: viscosity, fluid's type and composition, the size and amount of the solid particles contained in the drilling fluids, etc. (Schamp et al., 2006). Drilling fluids can thus either decrease or increase the mechanical friction depending on their specific properties. Generally, oil-based (OBM) and synthetic-based drilling fluids are used for the contact surfaces between the steel and rock, namely, the drillstring and wellbore. Such types of drilling fluids are referred to as nonaqueous-based drilling fluids (NADFs) which have higher lubricity effect compared to water-based drilling fluids (WBM) and thus provide lower values of friction coefficient when applied between the drillstring and borehole contact surfaces. Contrarily, WBMs tend to increase the mechanical

friction between the drillstring and borehole and consequently, lead to higher values of torque and drag (Growcock et al., 1999). Hence, it is important to bear in mind that the type of contact surface and the type and composition of the drilling fluids to which the contact surfaces are exposed, affect the friction coefficient values (Caenn et al., 2016; Growcock et al., 1999). Samuel (2010) reported the common friction coefficient values of different types of drilling fluids used by the industry for the open hole and cased hole sections of a well. Table 1.1 illustrates these values.

Table 1.1 Common friction coefficient ranges for different drilling fluids in the open hole and cased hole sections of a well (after Samuel (2010)).

Drillinf fluid type	Openhole friction coefficient	Cased hole friction coefficient
Oil-based	0.16-0.20	0.17-0.25
Water-based	0.25-0.35	0.25-0.40
Synthetic-based	0.12-0.18	0.15-0.25
Polymer-based	0.15-0.22	0.20-0.30
Brine	0.30-0.40	0.30-0.40
Air	0.35-0.55	0.40-0.60
Foam	0.30-0.40	0.35-0.55

Although NADFs offer sufficient lubricity, they also include several shortcomings such as high cost and environment-related issues. On the other hand, WBMs are often considered more environmentally friendly and cost efficient in comparison with NADFs. Therefore, there is a considerable requirement for WBMs with high performance and similar lubricity effect as NADFs (Breeden et al., 2011; Growcock et al., 1999; Redburn et al., 2013).

1.4.2.1 Lubricants used as drilling fluid additives

Mixing the drilling fluids with different additives, is one of the methods used in the industry to decrease the friction forces between the drillstring and the wellbore contact surfaces. However, this method has shown both successes and deficiencies in various operations (Redburn et al., 2013). Generally, there are two types of lubricants used as drilling fluid additives, namely, liquid type and solid type (Growcock et al., 1999; Sönmez et al., 2013). In the following sections, these two types of lubricants as well as their applicability and deficiencies are discussed.

1.4.2.1.1 Liquid lubricants

Generally, after being added to the drilling fluids, the liquid lubricants establish a tiny, thick layer of liquid which creates a space between the two surfaces in contact. The thick layer of liquid resists the high compressional forces and covers the contact surface roughness. Consequently, it can reduce the mechanical friction to an adequate amount (Growcock et al., 1999; Ismail et al., 2015; Ke and Foxenberg, 2010; Redburn et al., 2013). The liquid lubricants usually interact with the other components in the drilling fluid, which are surface-active. The efficiency of these lubricants is thus dependent on their concentration. Also, the absorption of such lubricants is prevented at high shear rates as they can become extremely stable and emulsified (Growcock et al., 1999). Among the liquid lubricants which are commercially used one can list: glyceride and fatty acid-based, polypropylene glycol-based and triglyceride and vegetable oil-based lubricants. In addition, in some locations, crude oil and diesel oil may be used as lubricants since they are considered cost-efficient and easy to access in the oil fields. However, they do not offer the same lubricity effect as the common commercial liquid lubricants (Sönmez et al., 2013).

Although the liquid lubricants have shown success in decreasing the mechanical friction and torque and drag, their efficiency is usually temporary and short-term. In addition, they may affect and change the properties of the drilling fluids. In general, the liquid lubricants are mostly effective during slug treatments and spot applications. This is because in such cases, the liquid lubricants are used as temporary solutions and they are thus able to sustain a liquid film with a certain strength between the contact surfaces. However, this effect can disappear after a short while since the liquid film is not strong enough to resist the high amount of forces applied in between the drillstring and borehole or casing contact surfaces. Also, as mentioned earlier, the liquid lubricants can lose their efficiency as they get highly emulsified due to high shear rates or due to the addition of chemicals which are required to sustain the properties of the drilling fluids (Redburn et al., 2013).

1.4.2.1.2 Solid lubricants

Solid materials such as plastic or glass beads which are added to the drilling fluids basically function as ball bearings between the drillstring and wellbore. The solid materials do not form any bonding with the contact surfaces with which they interact. Thereby, they are also not dependent on the drilling fluid type (Growcock et al., 1999; Redburn et al., 2013; Sönmez et al., 2013). These solid materials have shown success mostly in horizontal wells where hard and

smooth materials have been used. On the other hand, solid beads have also demonstrated some deficiencies which can lead to challenging situations. For instance, they can reduce in size due to the high velocity with which they are ejected through the bit nozzles. Also, the solid beads can be smashed in the space between the drillstring and the borehole or the casing and as a consequence, their surface area will be increased (Redburn et al., 2013). In addition, solid lubricants can lead to plugging issues with components of BHA (Schamp et al., 2006). Furthermore, the solid beads used during drilling operations increase the drilling fluids' expense. Also, the solid control equipment located at the surface eliminate a major portion of the beads (Redburn et al., 2013).

1.5 An overview of formerly used setup

To mitigate the mechanical friction in various operations during the lifetime of a well, the analysis of different parameters which may affect the friction coefficient in a wellbore is of great significance. Several researchers have considered certain parameters such as drilling fluid type and composition, surface roughness, applied load, temperature, etc. and analyzed their effect on the friction coefficient (Amanullah, 2016; Barraez et al., 2014; Kaarstad et al., 2009; Livescu et al., 2014; Patel et al., 2013; Quigley, 1989; Sönmez et al., 2013; Taghipour et al., 2014; Ytrehus et al., 2017). Different instruments or setup have been used to measure the effect of various parameters on the coefficient of friction. Each instrument may analyze only a certain number of parameters, as each instrument is design for a specific kind of test. In this section, the functionality of such instruments, the purpose of their use as well as their limitations have been discussed in detail.

1.5.1 Tribometer

Kaarstad et al. (2009) analyzed the effect of several water and oil-based drilling fluids on the coefficient of friction while parameters such as downhole temperature, contact surface roughness and applied load varied. For this purpose, they made use of a tribometer which is an instrument that works based on the technology of ball on disc. The tribometer could be controlled by a computer and had the ability to measure the friction coefficient of several drilling fluids with different properties. It also comprised a heating element, which made temperature measurements within the range of ambient temperature up to 150°C possible. However, Kaarstad et al. (2009) performed their tests within the temperature range of 10 to

100°C. Basalt, steel, chalk and concrete were also used as contact surfaces due to their similarity to some of the surfaces with which the drillstring is mostly in contact. A picture of the tribometer is shown in Fig. 1.4.
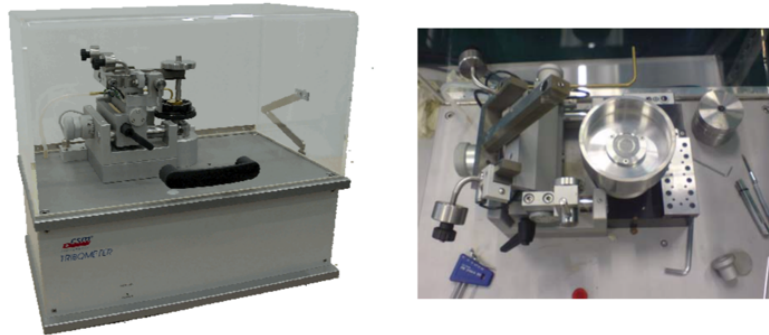
Fig. 1.4 Tribometer (after Kaarstad et al. (2009) and CMI instruments).

Further, Kaarstad et al. (2009) performed measurements of the friction coefficients of different drilling fluids with varying temperature and applied normal load. Based on their test results, they came to the conclusion that:

- The friction coefficient depends on contact surface roughness. For example, when the contact surfaces are steel and basalt, the friction coefficients are higher than when the contact surfaces are steel and steel.
- With increasing temperature, the friction coefficient also increases.
- The increase of applied load does not have a significant effect on the friction coefficient.

Despite the fact that the tribometer used in these experiments can measure the effect of different parameters on the friction coefficient simultaneously, it does not consider the effect of pressure on the friction coefficient. This can thus be considered as a limitation of this instrument.

1.5.2 Rotational and linear friction testers

As mentioned earlier, to reach the desirable target lateral length during the CT intervention operations, one of the simplest options to mitigate the mechanical friction is the use of lubricants (Livescu et al., 2014). To minimize CT's coefficient of friction, planning and designing the most optimum and efficient lubricant is quite essential. In an attempt to investigate the effect of different lubricants on CT friction coefficient, Livescu et al. (2014) used a rotational and a linear friction tester.

Generally, the rotational friction testers have been used for the purpose of performing measurements of the friction coefficients of CT lubricants at atmospheric conditions and then implementing the resulting values to downhole conditions for CT operations. The design of rotational friction testers makes them capable of simulating only the rotational motion of the drillstring and not the sliding, linear motion of the CT during the operations. Extreme Pressure (EP) and lubricity tester is a type of rotational friction tester and is manufactured by OFI Testing Equipment (OFITE), Inc. (OFITE, 2019a). Fig. 1.5 illustrates a picture of the EP and lubricity tester. This instrument includes a torque block which is made of steel and is pushed against a rotating ring which is also made of steel (Livescu et al., 2014). Basically, the EP and lubricity tester is designed to mimic the rotational speed of the drillstring and the pressure that the drillstring withstands while laying against the borehole wall. The instrument is most commonly used to measure the friction coefficient of different lubricants which are used as additives to the fluid. For a typical lubricity test, a moment as high as 150 in-pounds (i.e. about 17 N.m) is employed in between the steel torque block and the steel ring which is rotating at 60 rpm. This moment is equal to a pressure of 5000 to 10000 psi (i.e. about 345 to 690 bar) on the fluid in between the two contact surfaces. The instrument is also used to conduct extreme pressure test. Such a test is usually performed at shear rates as high as 1000 rpm. Also, the pressure of the fluid which is tested between the two steel contact surfaces can be within the range of 5000 to 100000 psi (i.e. about 345 to 690 bar) (Patel et al., 2013). Other types of rotational friction testers are usually based on other technologies like ball on disc or pin on disc (Livescu et al., 2014).

Barraez et al. (2014) also used the EP and lubricity tester to analyze the friction reducing features of different metal to metal lubricants particularly used for optimization of operations in ERWs. To measure the friction coefficients of various lubricants, they blended 14 lubricants in mixtures of fresh water and potassium chloride brine with specific friction reducer for fluids. These lubricants were typically used in the US fields such as Bakken and Eagle Ford. During their experiments, Barraez et al. evaluated the effect of pressure and fluid temperature on the friction coefficient of different lubricants. To investigate the effect of pressure, they considered high pressures within the range of 5000 to 10000 psi (i.e. about 345 to 690 bar) between the instruments' two metal contact surfaces which were in movement relative to each other. To examine the effect of temperature on the other hand, Barraez et al. had to warm up the lubricant solutions to certain downhole temperatures and then measure their corresponding friction coefficients at atmospheric temperature. This was done due to the limitation in the design of

the EP and lubricity tester, which does not include temperature measurements. Barraez et al. had not reported neither the downhole temperatures nor the time gap between adding the warmed up lubricant solutions and starting the friction tests. However, this time gap is particularly essential to make sure that the temperature of the fluids did not decrease when the friction coefficients were measured.

Fig. 1.5 EP and lubricity tester (after OFITE (2019a)).

Based on the results of the experiments with EP and Lubricity tester, Barraez et al. declared the reduction in the friction coefficients to be within the range of 45 to 78% which were verified by some field measurements of friction coefficients. However, they did not provide the exact values of the friction coefficients (Barraez et al., 2014; Livescu et al., 2014).

Livescu et al. (2014) also made use of the EP and lubricity tester to perform several rotational friction tests in order to measure the friction coefficient of three different CT lubricants. After running their tests at room conditions, they noticed a significant disagreement between the resulting values of friction coefficient obtained in the laboratory and the actual field values of friction coefficient. Livescu et al. explained the disagreement between the lab and field values of friction coefficient with the following three reasons:

1. The tests performed in the laboratory at atmospheric conditions should be as close to the conditions downhole as possible. This is because the downhole conditions such as temperature could have a considerable effect on fluid viscosity and chemical composition.

2. Generally, the rotational friction testers are not capable of reproducing the contact surfaces of the CT and the casing. Typically, the real values of the surface roughness of the CT and the casing can vary within the range of values below 1 and above 12 μm. However,

the rotational friction testers commonly give an average roughness of about 1 μm for the CT's and the casing's contact surfaces.

3. The rotational friction testers are not able to simulate the sliding, linear motion of the CT in the wellbore as they are designed based on ball on disc and pin on disc technologies (Livescu and Craig, 2014; Livescu et al., 2014).

Because of the above-mentioned reasons which led to the disagreement between the resulting laboratory values and the real field values of the CT coefficient of friction, Livescu et al. also made use of a linear friction tester to measure the linear, sliding friction coefficient of the CT.

The linear friction tester is an instrument designed to perform the same linear, sliding motion as the CT does while it is inside the well. A picture of the instrument is shown in Fig. 1.6.

Fig. 1.6 Linear friction tester (after Livescu et al. (2014)).

The linear friction tester is capable of measuring the friction coefficients of lubricants blended with the fluids downhole while parameters such as surface roughness, temperature and fluid composition and type change. The instrument makes it possible to use actual CT coupans which can be changed between the tests to prevent excessive wear. Also, actual samples of casing or metal plates with almost the same roughness as casing can be used in the instrument. Furthermore, the instrument has the capacity to hold various quantities of fluids with variable concentrations. For warming up the whole fluid system, CT and casing, a heating pad is placed beneath the metal plate upon which the CT coupan is moving. To control the temperature of

the entire system three thermocouples are implemented inside the instrument. The purpose of the thermocouples is to make sure that the temperature of the fluid is the same as the temperature of the two contact surfaces during each experiment. Livescu et al. performed the experiments using the linear friction tester with the temperature range of 20 to 98°C. During their experiments, the average surface roughness varied within the range of 0.92 to 10.23 μm for CT and 0.67 to 12.44 μm for casing. As reported by Livescu et al. (2014), in comparison with the rotational friction tester, the linear friction tester resulted in the friction coefficient values which were much closer to the actual field values.

Further, Livescu et. al concluded that the friction coefficient is mainly dependent on the temperature downhole, fluid type and composition and the contact surface roughness for instance between CT and casing. Also, particles such as sand, debris and proppant increase the contact surface roughness and consequently, enhance the friction coefficient (Livescu et al., 2014).

1.5.3 Lubricity Evaluation Monitor (LEM)

To measure the lubricity of various drilling fluids, the LEM series of lubricity evaluation monitors are often used. Fig. 1.7 shows a picture of this instrument. The design of such instruments makes them capable of performing static and dynamic experiments with drilling fluids as well as lubricants both at room and reservoir conditions. These instruments are able to conduct experiments both on core samples from the reservoir and different casing or drillpipe samples. Also, by simulating the surfaces of the wellbore and the tool joint as well as the reservoir conditions, the instruments give the user the possibility to measure the coefficient of friction or lubricity of the drilling fluid between the simulated surfaces and at simulated reservoir conditions. All the instruments from the series LEM have similar functionalities. They all include a mud test cell which includes a sample holder in which different samples such as limestone, sandstone, ceramic, quartz glass and field core or casing are inserted. A bob made of carbon steel which resembles the tool joint or the drill stem is implemented into the mud test cell. The bob can rotate at a desirable velocity. A load which is constant is then applied to the test sample and forces it towards the rotating bob. Further, both the axial load and the torque resulting from the rotating bob can be measured and evaluated. From this data, it is possible to find the torque as a function of friction or the axial load. Such measurements can be conducted as a function of temperature and pressure. Also, chemical additives can be later mixed with the

drilling fluid to estimate and analyze the variations in the friction factors (Patel et al., 2013; Quigley, 1989).

Fig. 1.7 Lubricity evaluation monitor- LEM series (after Corelab (2019)).

As discussed earlier, each of these mentioned setup or instruments have limitations and can only measure the effect of a certain number of parameters on the mechanical friction. Despite the various experimental research works on the effect of different parameters on the mechanical friction, there has not been much focus on the effect of pressure and its combined effect with temperature on the mechanical friction of different fluids. Therefore, in this study, a specially designed setup is used in combination with an automated high-pressure, high-temperature (HPHT) consistometer (OFITE, 2019b) in order to investigate the effect of pressure and temperature on the friction coefficient of different fluids. Further, the designed setup is explained in detail in section 3.1. In the following section, the overall objectives of this thesis work are listed.

2 PROJECT OBJECTIVES

In this thesis project, a setup was designed and used in combination with a HPHT consistometer from OFI Testing Equipment in order to achieve the following objectives:

- Investigating the challenges of the designed setup.
- Suggesting potential changes in the setup design for the optimization for future experiments.
- Performing experiments on four different fluids, namely, deionized water, mineral oil Calpar (100R) provided by OFI Testing Equipment (OFITE, 2010), oil-based (OBM) and water-based (WBM) drilling fluids.
- Investigating the effect of pressure and temperature on the friction coefficient of the four different fluids.
- Comparing the friction coefficient values of the four different fluids.

3 EXPERIMENTAL EQUIPMENT

In order to optimize the measurement of mechanical friction during different operations, various researches and experiments have been performed with the attempt to investigate the effect of several factors on the mechanical friction. However, the main focus has been on factors such as drilling fluid type and composition, contact surface roughness, downhole temperature, applied load, etc. On the other hand, there has not been much focus on investigating the effect of pressure and its combined effect with temperature on the mechanical friction. Therefore, in this study, the effect of pressure and temperature have been studied on the friction coefficient of four different fluids, namely, deionized water, mineral oil, OBM and WBM. For this purpose, an experimental setup has been designed and constructed at the University of Stavanger. The setup design was inspired by the work of Holand et al. (2007). To measure the friction coefficient of different drilling fluids and lubricants under downhole pressure and temperature conditions, Holand et al. (2007) made use of a setup which included a slurry cup and three pistons which were operated hydraulically. The three pistons were hydraulically pushed towards the wall of the slurry cup to generate normal force. The setup was then placed inside a HPHT consistometer's test cell and the hydraulically operated pistons were connected to a torque measurement device. However, the detailed working mechanism of this setup is not explained in the work of Holand et al. (2007). On the other hand, the experimental setup used in this thesis project includes a slurry cup and a metal shaft with three steel paddles which are operated mechanically. The following section explains this setup in detail.

3.1 Experimental setup

As mentioned earlier, for the purpose of the experiments in this project, a setup has been designed and constructed which is employed in a HPHT consistometer. Fig. 3.1 illustrates the different components of the setup.
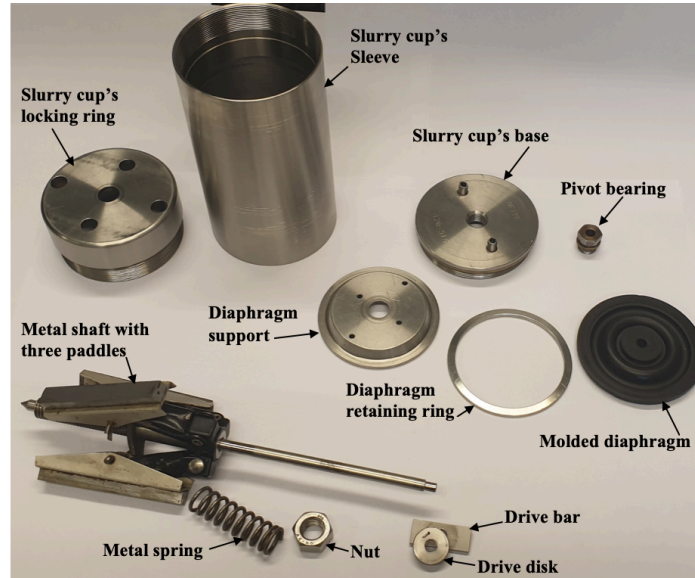
Fig. 3.1 Different components of the designed setup.

The setup comprises a steel slurry cup which is basically a test cell for holding the test fluid. The setup also includes a metal shaft which contains three steel paddles, a spring and a nut. The spring and the nut are used to apply normal force between the paddles and the inside wall of the slurry cup. By manually tightening the nut, the spring is pressed down, and the paddles will get closer to the slurry cup's wall. The closer the paddles are to the wall, the higher the friction force between the paddles and the wall will be. The paddles and the slurry cup's wall resemble the contact surfaces of the drillstring and the casing, respectively. When the metal shaft is located inside the test cell, the nut shall be tightened in such a way that the paddles can rotate freely without being stuck to the wall. In fact, the system is adjusted to a reference force when the slurry cup is empty. After calibration, the slurry cup is filled with the test fluid. Fig. 3.2 shows a picture of the metal shaft assembly and how it is placed inside the slurry cup.
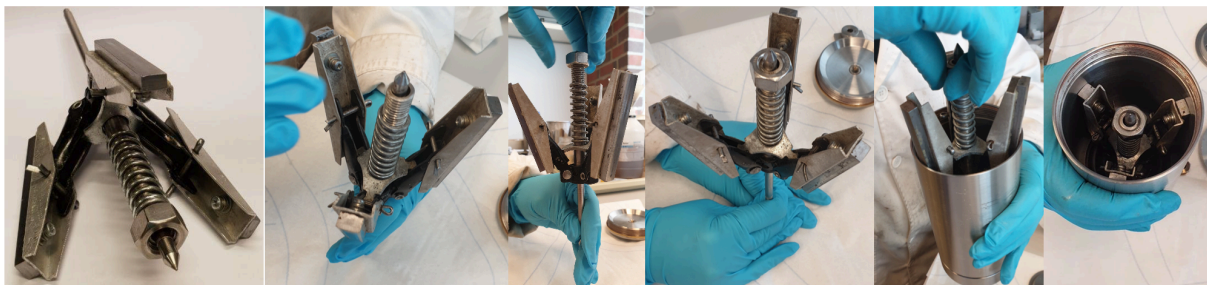
Fig. 3.2 The metal shaft with three paddles, a spring and a nut. The spring and the nut are used to apply normal force between the paddles and the inside wall of the slurry cup. The pictures from left to right show how the metal shaft assembly is placed inside the slurry cup.

The metal shaft exits from a hole at the bottom of the slurry cup and is tightened with a drive bar and a drive disk that are attached together with a small pin. It is essential that the drive bar and the drive disk are tightened in place with a tiny distance from the bottom of the slurry cup. This is because the instrument's potentiometer, which will be explained later in this section, needs to make contact with the drive bar to be able to measure the torque of the test fluid. Once the metal shaft is securely fixed in place, the test fluid can be poured into the slurry cup. It is important to make sure that there is no leak from any parts of the slurry cup. Therefore, at first, the test fluid is poured into the slurry cup up to a certain level. The slurry cup is then completely closed and sealed with a metal base which includes a hole on its top. The rest of the test fluid is then poured into the slurry cup by means of a funnel through the hole on the metal base. The hole is then securely sealed with a pivot bearing. Afterwards, the slurry cup is grabbed at its bottom by the use of lift tongs and placed inside the test cell of the HPHT consistometer. Fig. 3.3 illustrates the procedure of preparing the setup to be inserted into the HPHT consistometer.

Fig. 3.3 The procedure of preparing the setup to be inserted into the HPHT consistometer.

Once the slurry cup is in place, a potentiometer is implemented on top of the slurry cup. The potentiometer is in contact with the drive bar at the bottom of the metal shaft and is capable of measuring the output voltage of the test fluid which has a direct proportionality with the amount of torque that the test fluid applies on the setup paddles. When the potentiometer is perfectly in its position, the consistometer's cell cap can be closed and the test can be run (OFITE, 2019b). Fig. 3.4 shows pictures of the potentiometer as well as the procedure of placing the setup inside the consistometer's test cell and making the instrument ready for the experiments.
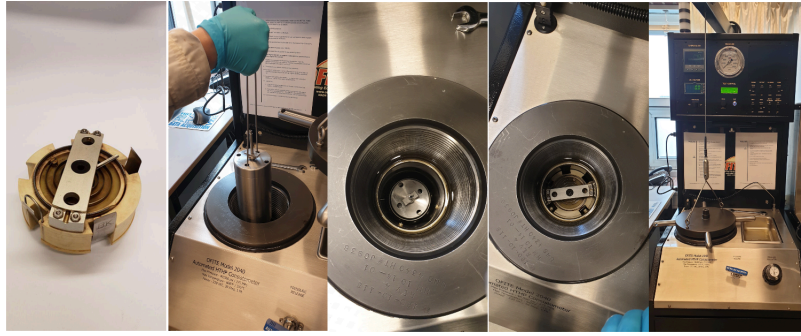
Fig. 3.4 From left to right, the pictures show the potentiometer, the lift tongs which are used to grab the setup and place it into the consistometer's test cell, the setup which is correctly in place, the potentiometer which is implemented on top of the setup, the consistometer's cell cap which is closed and the instrument which is ready for starting the experiments.

The automated HPHT consistometer is computer controlled and includes a software which makes it possible to define the desired temperature and pressure for each experiment. The software not only monitors the instrument but also measures and records pressure, temperature and the consistency of the test fluid and simultaneously plots these data versus time during each experiment. Fig. 3.5 shows the automated HPHT consistometer as well as its software.
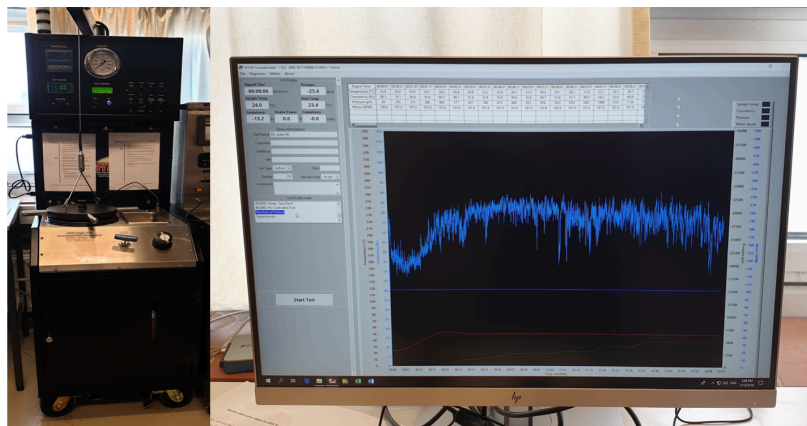
Fig. 3.5 Automated HPHT consistometer and its software

3.2 Pressure and temperature settings for each experiment

In this study, four different fluids were analyzed using the designed setup and the HPHT consistometer. These fluids include deionized water, mineral oil Calpar 100R from OFI Testing Equipment (OFITE, 2010), OBM and WBM which were prepared in the drilling fluid laboratory at the University of Stavanger. The effects of pressure, temperature and fluid type on the friction coefficient of the four fluids were then investigated during several experiments.

Since the designed setup was still in the optimization phase, it was decided to investigate the mechanical friction coefficient of the different fluids, only between steel on steel contact surfaces, namely, the slurry cup's wall and the three paddles. As mentioned earlier, the contact surfaces simulate the contact between the rotating drillstring and the casing. The fluids were poured into the slurry cup and the setup was prepared to be inserted into the HPHT consistometer according to the procedure explained in section 3.1. For each fluid ten experiments were performed. Five experiments were done at a constant temperature of 25°C and five at a constant temperature of 50°C. For both series of experiments, the pressure was increased up to 5000 psi (345 bar). The settings of the HPHT consistometer were adjusted according to the target temperatures and pressures. Table 3.1 illustrates the target sample temperatures as well as the ramp-up time required to achieve the temperatures and the require hold-time to keep the sample temperature constant for each experiment. Table 3.2 shows the steps to ramp up the pressure as well as the require hold-time for each pressure step.

Table 3.1 Target sample temperatures set for the experiments performed on each fluid.

Target temperature (°C)	Ramp time (min)	Hold time (min)
25	1	895
50	10	895

Table 3.2 Pressure increase steps set for the five experiments performed on each fluid at each temperature.

Steps	Ramp time (min)	Target pressure (psi)	Target pressure (bar)	Hold time (min)
1	3	1000	69	30
2	3	2000	138	30
3	3	3000	207	30
4	3	4000	276	30
5	3	5000	345	30

The rotational speed with which the setup's metal shaft rotated, was adjusted according to the best-practice values used in the industry during the drilling operations. These values are used as guidelines for drilling of different hole sections. Table 3.3 shows the values of common flowrates in liters per minute (lpm) as well as the rotational speed in rotation per minute (rpm).

Table 3.3 Common flowrate and rotational speed values used by the industry for drilling of different hole sections.

Hole size (inch)	17 1/2"	16"	12 1/4"	9 1/2"	8 1/2"
Flow rate (lpm)	>4500	>4100	>3000	>2100	>1800
Rotation (rpm)	>150	>150	>120	>130	>120

To estimate the required rotational speed for the experiments, an extrapolation was performed using the rotational speed data for 17 ½" and 8 ½" hole sections. The slurry cup's diameter was measured and set as 2.93". The required rotational speed was then calculated using Eq. 2.

$$RPM_{Setup} = RPM_1 + \frac{D - D_1}{D_2 - D_1} \ (RPM_2 - RPM_1) \qquad (2)$$

where,

- RPM_{Setup} is the required rotational speed for the setup which should be calculated.

- RPM_1 and RPM_2 are the common values used for hole sections 17 ½" and 8 ½", respectively.

- D is the slurry cup's diameter which is 2.93".

- D_1 and D_2 are the 17 ½" and 8 ½" hole diameter values, respectively.

The calculated rotational speed was 101 rpm and was kept constant for all the experiments. The total time taken for each set of five tests at 25°C was estimated to be 14 hours and 56 minutes and for each five tests performed at 50°C, the total time was estimated to be approximately 15 hours and 5 minutes. Primarily, the purpose was to run each set of five tests in one run. However, the HPHT consistometer automatically stopped after running for three tests. After the tests were stopped, the slurry cup was removed from the consistometer's test cell to investigate the issue. It was observed that the drive bar and the drive disk were attached to the bottom of the slurry cup (slurry cup's locking ring) as shown in Fig. 3.6. The drive bar should be in contact with the instrument's potentiometer in order to transfer the fluid torque such that the potentiometer can display the torque in the form of consistency. However, when this connection is interrupted, the potentiometer cannot measure the fluid torque and thereby, the tests stop.

Fig. 3.6 The drive disk and the drive bar attached to the bottom of the slurry cup or the slurry cup's locking ring.

Therefore, it was decided to take three tests in one run and two tests in another run for each temperature. In this way, the reliability of the data and reproducibility of results could be examined when starting the experiments from initial conditions again. The reasons behind repeating a test five times with the same temperature and pressure conditions were the following:

- To detect the issues and the uncertainties with the designed setup.

- To obtain reliable trends for the coefficient of friction of different fluids.

- To be able to observe the effect of pressure and temperature on the friction coefficient of the different fluids.

3.3 Setup challenges

The designed setup faced several challenges during the experiments. It was essential to detect these challenges and find methods to mitigate them to be able to run all the experiments. In this section, different challenges as well as their mitigation methods are addressed.

- Large variations in the consistency values of each fluid occurred due to the instability of the paddles and fluctuations of the metal shaft. Consequently, this issue affected the friction coefficient trend for each fluid as consistency has direct proportionality with the fluid torque.

- The repetition of each experiment five times with the same temperature and pressure conditions could help to obtain more reliable and reasonable trends of friction coefficient for each fluid.

- Sudden interruptions of the tests happened due to the loss of contact between the potentiometer and the setup's drive bar (see the previous section).
  - Each time the tests were interrupted, the slurry cup was removed from the test cell of the HPHT consistometer. The drive disk and the drive bar were then fixed in place with a tiny distance from the bottom of the slurry cup.

- The nut used to adjust the normal force applied between the paddles and the slurry cup's wall, was unstable and thus its position had to be adjusted for each experiment.
  - To solve this issue, the position of the nut was adjusted such that when the dry setup (with no fluid inside) was inserted into the HPHT consistometer, the potentiometer could read an output voltage value of 3.5 volts and a consistency value within the range of 15 to 20 Bc.

- Although the temperatures were set to be constant, they increased by 2 to 5°C during the experiments. This happened because of the mechanical friction between the paddles and the slurry cup's wall, particularly when OBM and WBM were used as test fluids.
  - The temperature variations were neglected since the mechanical friction between the paddles and the slurry cup's wall was unavoidable. Also, the variations were negligible since the target temperatures were only increased by 2 to 5°C. However, these variations were measured.

- After performing all the experiments, it was observed that the inside wall of the slurry cup and the surface of the paddles were scratched and worn out. This may have slightly affected the results since the surface roughness of the two contact surfaces might have changed due to continuous scratching and wear during the experiments. Fig. 3.7 shows the worn-out surface of the used slurry cup versus a new slurry cup. Also, Fig. 3.8 illustrates the eroded surface of the setup paddles after the experiments.

- o Nonetheless, it was decided to perform all the experiments in this project with the same slurry cup and setup paddles to maintain the same experimental conditions during all the experiments.
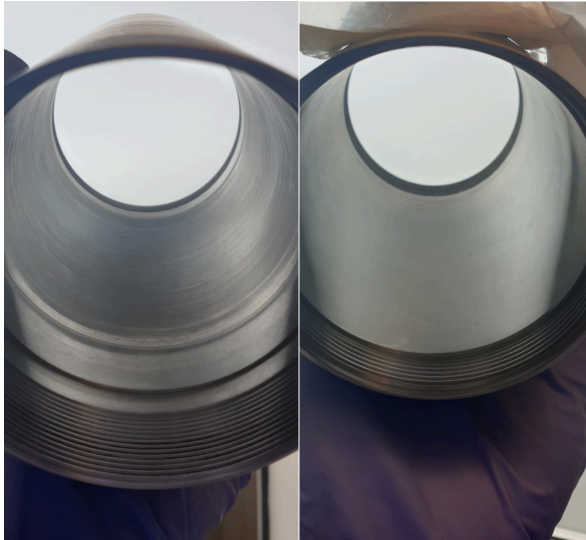
Fig. 3.7 Comparison of a used slurry cup with a new one. The picture on the left shows the used slurry cup with a worn-out inside wall after the experiments while the picture on the right shows a new slurry cup.

Fig. 3.8 A picture of the eroded surfaces of the three setup paddles after the experiments.

3.4 Suggestions for optimization of the setup

Each newly designed instrument or setup requires optimization in order for it to be applicable and be able to achieve reliable results. Based on the challenges that were discussed in the previous section, relevant suggestions are proposed that should be taken into consideration to improve the setup design and consequently, its applicability for future experiments.

1. The length of the setup's paddles should be decreased by 50%. Reducing the length of the paddles can decrease their axial movement and fluctuation during the experiments. This will help to lessen the large variations in the measured torque values.

2. The position of the setup's nut should be fixed such that it does not need adjustments before each experiment. This can be done by the help of a torque reader or by welding the nut at a certain position such that when the setup is inserted into the consistometer, the instrument's potentiometer can read an output voltage of 3.5 volts or a consistency value within the range of 15 to 20 Bc. This can lead to more reliable results.

3. Since the drive disk and the drive bar should be fixed with a tiny distance from the bottom of the slurry cup to be able to be in contact with the potentiometer, it is necessary to mark their exact position on the setup's metal shaft such that they can be tightened at the same position for every experiment.

4. The slurry cup and setup paddles should be changed after each experiment or after they are used for a few experiments as their contact surfaces may be scratched and eroded during continuous use (See Fig. 3.7 and Fig. 3.8). As a consequence, the surface roughness of the slurry cup's inside wall and the three paddles may change and affect the results of the experiments.

3.5 Analytical approach

As mention in section 3.1, during the experiments, the HPHT consistometer measures and records consistency values of the test fluid. The consistency values are directly proportional to the torque that the test fluids apply to the setup paddles. After each experiment, the recorded consistency values were thus converted to torque values using Eq. 3 which is extracted from API recommended practice 10B-2 (API, 2013).

$$T = 78.2 + (20.2 \times B_c) \tag{3}$$

where,

T is the torque in gram-centimeters (g.cm) and B_c is the consistency in Bearden units. The torque unit was then changed to Newton-meters (N.m) since it was decided to use SI units in all the calculations. In order to convert the torque values to friction coefficient, the following approach was used.

For each paddle of the setup, the torque can be defined as:

$$T = F \times R = \mu \times N \times R \tag{4}$$

where,

- T is the torque in Newton-meters (N.m).

- F is the friction force applied on each paddle in Newton (N), which can be defined as μ, the friction coefficient of each fluid multiplied by N, the normal force inserted on each paddle.

- R is the torque arm or the radius of the slurry cup in meters (m) (see Fig. 3.9).
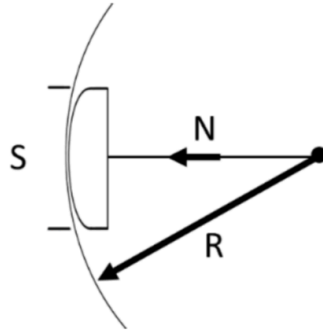
Fig. 3.9 The sketch shows the radius of the slurry cup and the normal force applied on each paddle.

The total torque applied on the three paddles can thus be defined as:

$$T_T = 3\mu \times N \times R \tag{5}$$

To apply normal load on the setup's paddles, two measurement concepts can be used, namely, direct and indirect concepts. The direct measurement concept makes use of hydraulic pressure to apply normal force on the paddles (see Fig. 3.10). However, due to manufacturing challenges, this concept was not selected for the design of the setup used in this project. Instead, the indirect measurement concept was used.
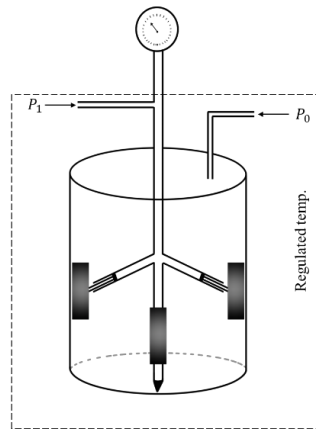
Fig. 3.10 Sketch of the setup design with the direct measurement concept. Hydraulic pressure applies normal force on the paddles.

The indirect measurement concept uses mechanical pressure to apply normal force on the paddles. The mechanical pressure is created by the use of the metal spring which is implemented in the setup. Fig. 3.11 shows a sketch of the indirect concept used in the design of the setup.
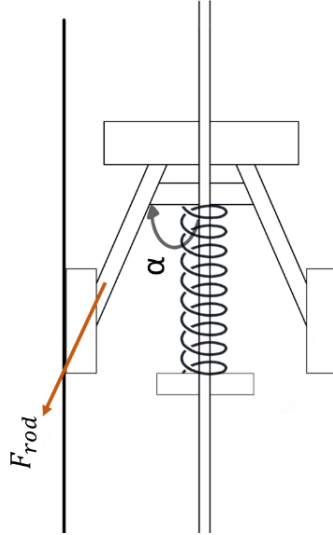
Fig. 3.11 Sketch of the setup design with the indirect measurement concept. The metal spring generates mechanical pressure which applies normal force on the paddles.

To calculate the normal force applied on the paddles, firstly, the spring force should be calculated. The spring force can be defined as:

$$F_K = Kx \tag{6}$$

where,

F_K is the spring force in Newton (N), K is the spring constant in Newton per millimeter (N/mm) which is a function of temperature (K=K(T)) and x is the spring displacement in millimeter (mm).

3.5.1 Spring constant measurements

To estimate the spring constant, several experiments were performed on the metal spring at different temperatures and applied loads. For this purpose, the metal spring was placed inside a thermocup filled with water (OFITE, 2019c). The thermocup makes it possible to vary the temperature of the water and consequently, that of the spring. The thermocup was then placed under a uniaxial compressive strength tester (UCS) which applies different loads on the spring

and has the ability to record the applied loads and plot them versus the spring deformation. A picture of the thermocup and the UCS tester is shown in Fig. 3.12.
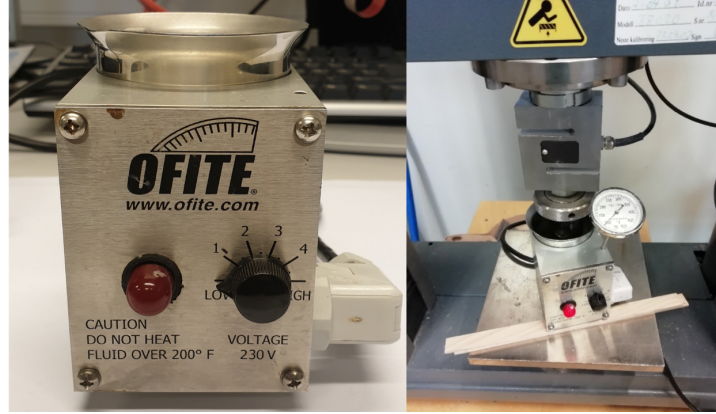
Fig. 3.12 The thermocup and the UCS tester used to measure the spring constant at different temperatures and applied loads (OFITE, 2019c).

Five experiments were performed on the metal spring at temperatures of 20, 30, 40, 50 and 60°C, respectively. For each temperature, the applied force on the spring was increased up to 50 N. The UCS tester then generated five plots of applied load versus spring deformation for the five experiments (see Fig. 8.1 to Fig. 8.5 in section 8.1). The slopes of the plots were computed using the trend line function in Excel and showed the spring constant values at each specified temperature. Table 3.4 shows the spring constant values at each temperature.

Table 3.4 The spring constants values at each temperature.

Temperature (°C)	Spring constant (N/mm)
20	7.13
30	7.24
40	7.29
50	7.34
60	7.42

Further, the spring constant values were plotted versus temperature (see Fig. 3.13). By applying a trend line on the spring constant values, the following polynomial equation was generated for the spring constant as a function of temperature:

$$K(T) = 10^{-5}\, T^3 - 0.0015\, T^2 + 0.0657\, T + 6.2806 \qquad (7)$$
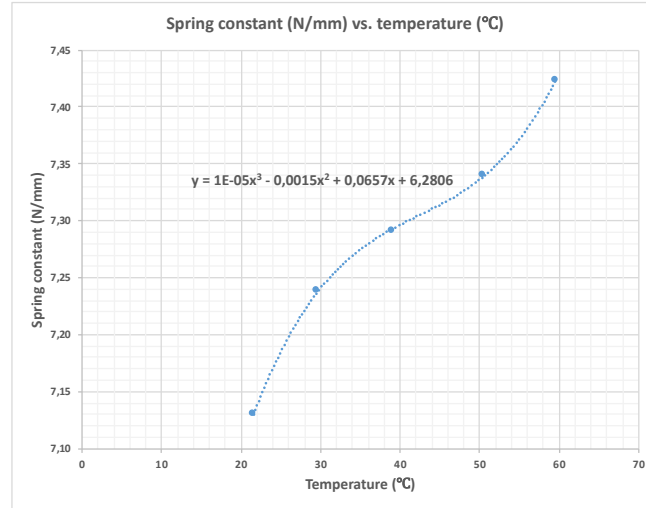
Fig. 3.13 The plot of the spring constant versus temperature. A polynomial equation is generated for the spring constant as a function of temperature.

To find the spring displacement, the original length of the spring before it was placed in the setup, was measured to be 50.11 mm. After the spring was inserted in the setup and the nut was tightened, the length of the spring was changed to 49.59 mm. The spring displacement was thus the difference between the spring's original length and final length after it was place in the setup. Thereby, the spring displacement was 0.52 mm and was kept constant during all the experiments.

As shown in Fig. 3.11, the force employed on each paddle in the axial direction can be defined as:

$$F_P = F_{rod} \cos\alpha = \frac{1}{3} F_K \tag{8}$$

where,

F_P is the force employed on each paddle, F_{rod} is the force that the metal rod applies on each paddle and α is the angle that each paddle makes with the vertical axis. The force exerted on each paddle is also equal to one third of the spring force ($\frac{1}{3}F_K$).

Therefore,

$$F_{rod} = \frac{F_K}{3cos\alpha} \tag{9}$$

Then, the normal force exerted on each paddle can be calculated as:

$$N = F_{rod}\sin\alpha = \frac{F_K}{3}\tan\alpha \tag{10}$$

Once the normal force is computed, the friction coefficient can be calculated using Eq. 5. By solving Eq. 5 for the coefficient of friction, Eq. 11 is generated.

$$\mu = \frac{T_T}{3 \times N \times R} \tag{11}$$

Therefore, this analytical approach was used to calculate the friction coefficient for all the experiments and Eqs. 3 to 11 were used in all the calculations. After performing each series of experiments, the results were sorted in the following manner:

1. The recorded consistency values of each fluid provided by the HPHT consistometer, were converted to torque values using Eq. 3.
2. The normal force was then computed using Eqs. 7 to 10.
3. The friction coefficient was calculated using Eq. 11.

4 RESULTS AND DISCUSSION

As mentioned in section 3.2, four fluids: deionized water, mineral oil Calpar (100R), OBM and WBM were studied with respect to their effect on the mechanical friction between the two steel contact surfaces using the specially designed setup. The experiments were designed to measure the effect of pressure and temperature on the friction coefficient. In this section the results obtained for each fluid will be presented and argued in detail.

4.1 Data handling

Five repeated experiments with the same temperature, pressure and rotational speed conditions were performed on each fluid (see Table 3.1 to Table 3.3). The repetition of the experiments was essential due to the setup challenges explained in section 3.3. After each experiment, the consistency values of each fluid recorded by the HPHT consistometer's software, were first converted to torque values and then to friction coefficient values using the analytical approach explained in section 3.5.

For each experiment, due to the large amount of data, it was decided to take average values of the pressure and friction coefficient data for each pressure step. The averaged data were then used to generate plots of friction coefficient versus pressure. Five curves of friction coefficient versus pressure were then generated in the same plot. This helped to identify the outlier trends, in general two per repeated experiment, which were mainly caused by the experimental challenges described in section 3.3. Because of this, out of the generated five curves, three which showed similar trends of friction coefficient versus pressure were selected. Finally, to obtain a single trend, the friction coefficient and pressure data of the selected three curves were averaged. Also, the standard deviations of the averaged data of the three curves were computed to consider how the differences among the measured trends were significative with respect to the accuracy of the measurements. This approach was used to handle the resulting data from each experiment. In the following section, the results obtained for each fluid will be discussed in detail.

4.2 Deionized water

4.2.1 The effect of pressure on the friction coefficient

Fig. 4.1 shows the three selected curves at the temperature of 25℃ and Fig. 4.2 illustrates the single average trend of friction coefficient versus pressure as well as the standard deviations of the averaged data.

Similarly, Fig. 4.3 and Fig. 4.4 show the same data for the measurements at 50℃. Finally, Table 4.1 reports the corresponding numerical values.

Fig. 4.1 Three selected curves with similar trends. The curves show the variation of the friction coefficient of deionized water with increasing pressure at constant temperature of 25℃.

Fig. 4.2 A single trend showing the variation of friction coefficient of deionized water with increasing pressure at constant temperature of 25℃. The red error bars show the standard deviation of the averaged data.

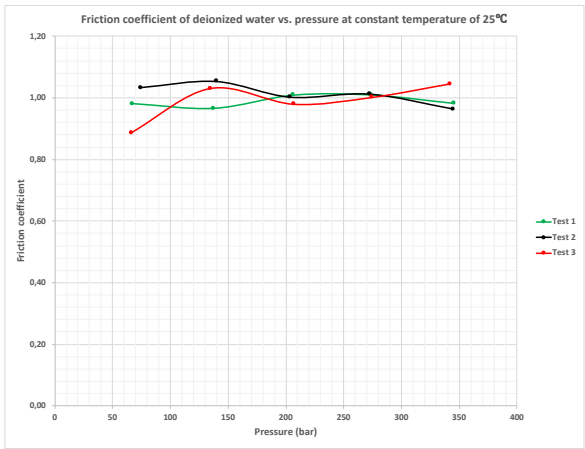**Fig. 4.3** Three selected curves with similar trends. The curves show the variationf of the friction coefficient of deionized water with increasing pressure at constant temperature of 50℃.
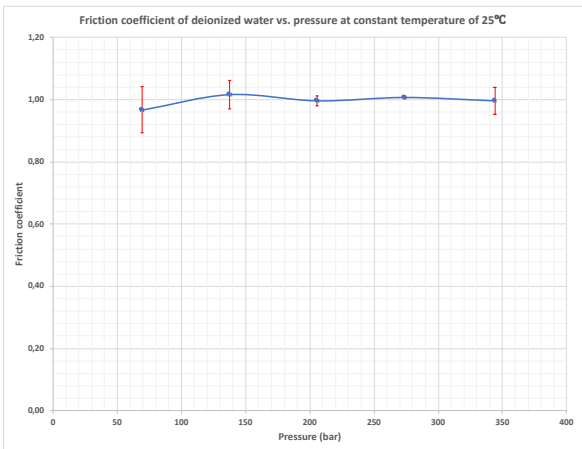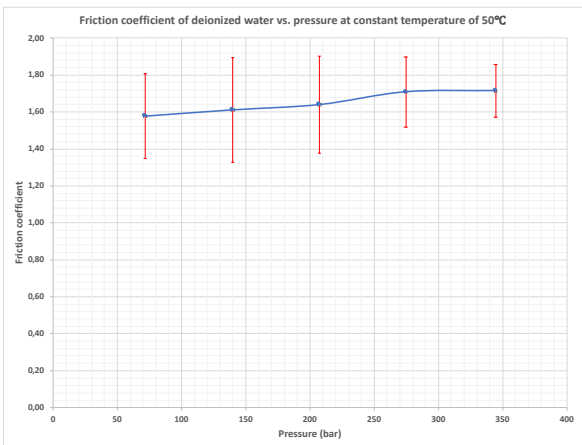

Fig. 4.4 A single trend showing the variation of friction coefficient of deionized water with increasing pressure at constant temperature of 50℃. The red error bars show the standard deviation of the averaged data.
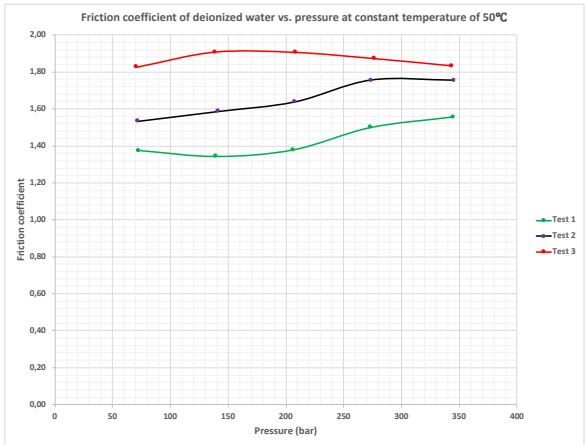
Table 4.1 Friction coefficient values of deionized water at constant temperatures of 25 and 50°C and increasing pressure up to 345 bar.

Deionized water		
Pressure (bar)	Friction coefficient at 25°C	Friction coefficient at 50°C
69	0.97	1.58
138	1.02	1.61
207	1.00	1.64
276	1.01	1.71
345	1.00	1.71

As it can be observed from Fig. 4.2, the friction coefficient of deionized water was measured to have almost a constant value of about 1 with increasing pressure at constant temperature of 25°C.

When the temperature is kept constant at 50°C, as it can be seen from Fig. 4.4, the friction coefficient of deionized water increases with increasing pressure, with an increase by about 9% from a value of 1.58 at the pressure of 69 bar to a value of 1.71 at the pressure of 345 bar.

In principle, the change of viscosity of deionized water with temperature and pressure is the main factor to justify the changes in the measured friction factor. To verify this assumption, a literature review was performed on the subject: this led to considering two studies by Bridgman (1949) and Wonham (1967) in which the effect of pressure on the viscosity of water was investigated. The main results in these studies showed that at temperatures above 33°C, the viscosity of water increases with increasing pressure while at temperatures below this value, water's viscosity gradually decreases with increasing pressure and reaches a minimum value at elevated pressures as high as 980 bar. The decrease in water's viscosity occurs because of the destruction in the molecular structure of water at such extremely high pressures (Bridgman, 1949; Wonham, 1967).

This experimental evidence can be used to interpret the results obtained during the experiments with deionized water. As observed in Fig. 4.2, the friction coefficient of deionized water was approximately constant with increasing pressure at constant temperature of 25°C. This observation is not in agreement with the results published by Bridgman (1949) and Wonham (1967), as a decrease of the friction coefficient with increasing pressure should have been expected at temperatures below 33°C. This difference could be explained by the following two reasons:

1. Due to setup challenges, such as sudden movements of the setup paddles during the experiments, the friction coefficient values of deionized water may be higher than expected.

2. At temperatures below 33°C, the effect of pressure on water's viscosity may be noticeable only at extremely elevated pressures, namely, pressures as high as 980 bar. Since the pressure was only raised up to 345 bar during the experiments, its effect on the viscosity and consequently, the friction coefficient of deionized water may not be significant at constant temperature of 25°C.

The results from the experiments at constant temperature of 50°C, showed that the friction coefficient of deionized water increases by 9% with increasing pressure (see Fig. 4.4 and Table 4.1). The increasing trend of friction coefficient is in agreement with Bridgman and Wonham's observations: as the viscosity of deionized water increases with increasing pressure at temperatures above 33°C (in this case at 50°C), the lubricity effect of deionized water also decreases, which leads to an increase in its friction coefficient.

4.2.2 The effect of temperature on the friction coefficient

The effect of temperature on the friction coefficient of deionized water is shown in Fig. 4.5. As it can be seen, the friction coefficient values of deionized water at constant temperature of 50°C are systematically larger than those at constant temperature of 25°C. Table 4.2 shows the corresponding numerical data and provides the percentage increase in the friction coefficient values of deionized water as the temperature changes from 25 to 50°C at each pressure step.
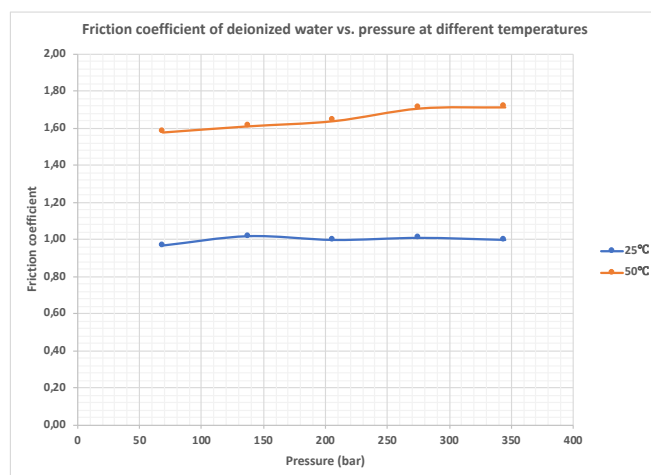
Fig. 4.5 Comparison of the friction coefficient values of deionized water at temperatures of 25 and 50°C.

Table 4.2 Percentage increase in friction coefficient of deionized water as the temperature changes from 25 to 50°C at each pressure step.

Deionized water			
Pressure (bar)	**Friction coefficient at 25°C**	**Friction coefficient at 50°C**	**% Increase in friction coefficient**
69	0.97	1.58	63
138	1.02	1.61	58
207	1.00	1.64	64
276	1.01	1.71	69
345	1.00	1.71	71

Generally, the viscosity of liquid water decreases with increasing temperature (Beal, 1946). Hence, a decrease of the friction coefficient of the deionized water should be expected with the increase in temperature. However, the results of the experiments show an opposite behavior, where the values of the friction coefficient are about 65% larger at the temperature of 50°C compared to the values at temperature of 25°C. This behavior could be caused by the experimental challenges explained in section 3.3.

4.3 Mineral oil Calpar (100R)

4.3.1 The effect of pressure on the friction coefficient

Five experiments were performed on mineral oil Calpar (100R) (OFITE, 2010) at constant temperature of 25°C while the pressure increased up to 345 bar. Fig. 4.6 illustrates the three selected curves of friction coefficient versus pressure, and Fig. 4.7 shows a single trend of the averaged friction coefficient and pressure data of the three curves and the standard deviations among the averaged data. Similarly, Fig. 4.8 and Fig. 4.9 show the same data for the measurements at 50°C. Finally, Table 4.3 reports the corresponding numerical values.
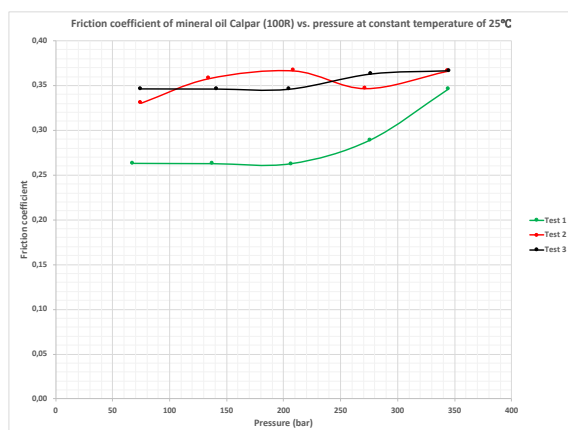
Fig. 4.6 Three selected curves with similar trends. The curves show the variation of the friction coefficient of mineral oil Calpar (100R) with increasing pressure at constant temperature of 25°C.
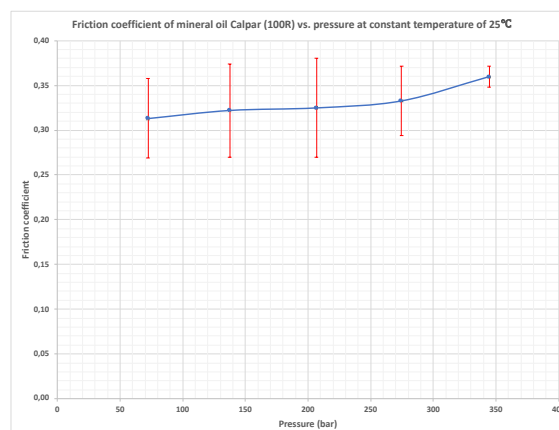
Fig. 4.7 A single trend showing the variation of friction coefficient of mineral oil Calpar (100R) with increasing pressure at constant temperature of 25°C. The red error bars show the standard deviation of the averaged data.
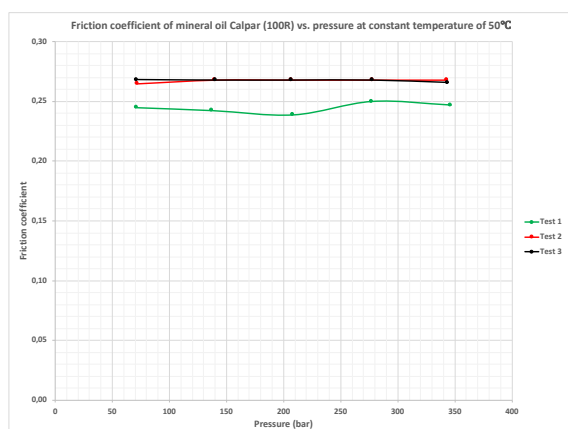
Fig. 4.8 Three selected curves with similar trends. The curves show the variation of the friction coefficient of mineral oil Calpar (100R) with increasing pressure at constant temperature of 50°C.
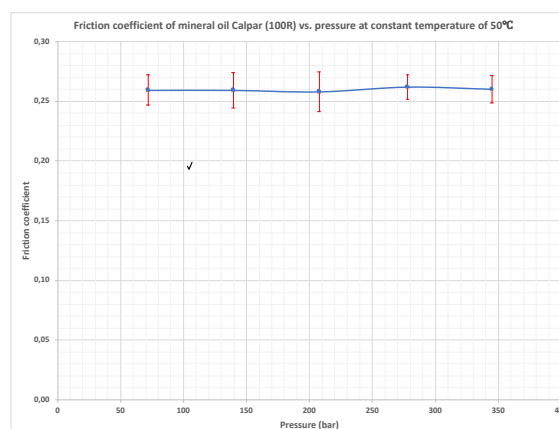
Fig. 4.9 A single trend showing the variation of friction coefficient of mineral oil Calpar (100R) with increasing pressure at constant temperature of 50°C. The red error bars show the standard deviation of the averaged data.

Table 4.3 Friction coefficient values of mineral oil Calpar (100R) at constant temperatures of 25 and 50°C and increasing pressure up to 345 bar.

Mineral oil Calpar (100R)		
Pressure (bar)	**Friction coefficient at 25°C**	**Friction coefficient at 50°C**
69	0.31	0.26
138	0.32	0.26
207	0.32	0.26
276	0.33	0.26
345	0.36	0.26

As it can be seen in Fig. 4.7, at constant temperature of 25℃, on average the friction coefficient of mineral oil increases with increasing pressure by 15% from a value of 0.31 at the pressure of 69 bar to a value of 0.36 at the pressure of 345 bar. However, since the standard deviation for most of the lower pressures is of the same order, one cannot exclude that this trend could be constant within the range of 0.27 to 0.37.

Instead, as it can be observed in Fig. 4.9, the friction coefficient values of mineral oil are almost constant and equal to 0.26 with an average standard deviation of ±1.32%.

Knežević and Savić (2006) performed a study on the effect of pressure and temperature on the viscosity of paraffinic mineral oils. In their study, it is discussed that the viscosity of mineral oil decreases rapidly with increasing temperature and that it increases with increasing pressure. Further, it is also mentioned that the chemical composition of the mineral oil has a strong effect on its viscosity-pressure relationship. Since the Calpar (100R) is a paraffinic mineral oil, the results obtained in this study can thus be interpreted based on the statements in Knežević's and Savić's study. Hence, the observed increase of the friction coefficient with pressure at constant temperature of 25℃ may be due to the increase of the viscosity of the mineral oil with increasing pressure and to the consequent decrease of its lubricity effect (see Fig. 4.7). Also, because of the same reason, an increasing trend of the friction coefficient of mineral oil with increasing pressure should be expected for the experiments performed at constant temperature of 50℃. However, the actual results in this case illustrate a constant trend of friction coefficient with increasing pressure (see Fig. 4.9). The constant trend obtained in this case could be due to the combined effect of pressure and temperature. However, the temperature seems to have a more dominating effect on the friction coefficient.

4.3.2 The effect of temperature on the friction coefficient

Fig. 4.10 illustrates the effect of temperature on the friction coefficient of the mineral oil. Also, Table 4.4 shows the corresponding numerical data and provides the percentage decrease in the friction coefficient values of the mineral oil as the temperature changes from 25 to 50℃ at each pressure step. As it can be observed, the friction coefficient values of the mineral oil at constant temperature of 50℃ are lower with respect to the values at constant temperature of 25℃ (about an average of -20% at most of the pressures and -28% at 345 bar). This is the expected behavior according to the study by Knežević and Savić (2006), due to the decrease of the viscosity of mineral oil with increasing temperature.
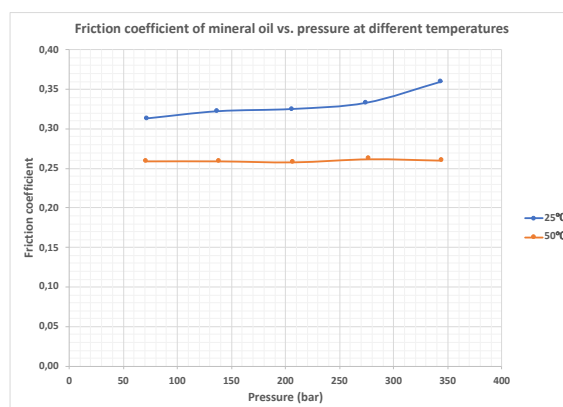
Fig. 4.10 Comparison of the friction coefficient values of mineral oil Calpar (100R) at temperatures of 25 and 50°C.

Table 4.4 Percentage decrease in friction coefficient of the mineral oil as the temperature changes from 25 to 50°C at each pressure step.

Mineral oil Calpar (100R)			
Pressure (bar)	Friction coefficient at 25°C	Friction coefficient at 50°C	% Decrease in friction coefficient
69	0.31	0.26	-17
138	0.32	0.26	-19
207	0.32	0.26	-21
276	0.33	0.26	-21
345	0.36	0.26	-28

4.4 Oil-based drilling fluid (OBM)

The OBM was prepared in the drilling fluid laboratory at the University of Stavanger. Table 4.5 lists its composition.

Table 4.5 The composition of the OBM.

Materials	Quantity	Unit
Base oil (EDC 95/11)	206	ml
$CaCl_2$ solution	60	ml
Emulgator, One-Mul	10	ml
$Ca(OH)_2$	8.5	g
Organophilic clay	5.5	g
Versatrol M	6	g
Barite	115	g

4.4.1 The effect of pressure on the friction coefficient

Five experiments were performed on the OBM at 25℃ with increasing pressure up to 345 bar. Fig. 4.11 shows the three selected curves of the OBM's friction coefficient versus pressure. Also, Fig. 4.12 shows a single trend of the averaged friction coefficient and pressure data of the three curves as well as the standard deviations among the averaged data. Similarly, Fig. 4.13 and Fig. 4.14 show the same data for the measurements at 50℃. Finally, Table 4.6 reports the corresponding numerical values.
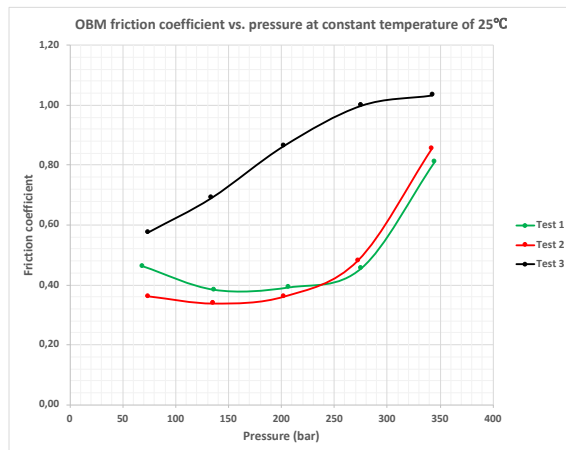
Fig. 4.11 Three selected curves with similar trends. The curves show the variation of the friction coefficient of OBM with increasing pressure at constant temperature of 25°C.
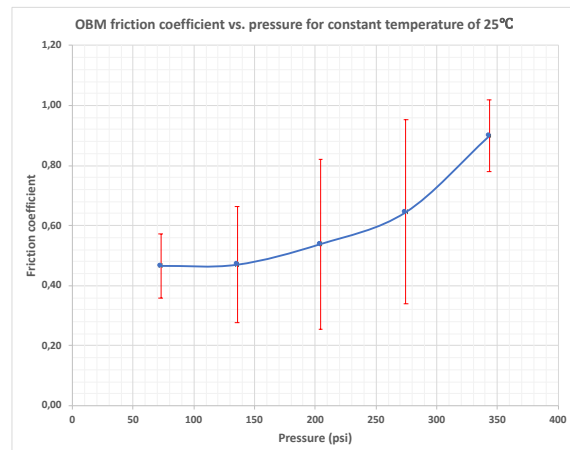
Fig. 4.12 A single trend showing the variation of friction coefficient of OBM with increasing pressure at constant temperature of 25°C. The red error bars show the standard deviation of the averaged data.
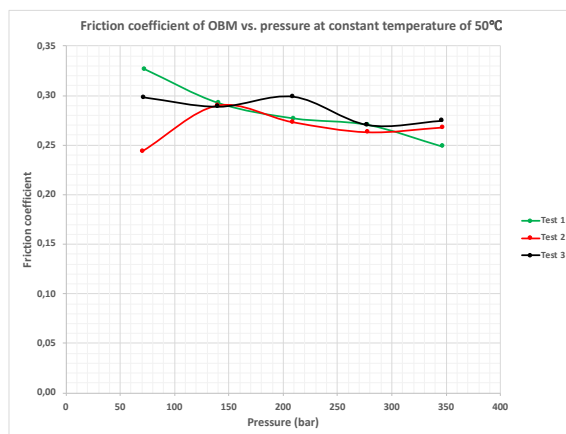
Fig. 4.13 Three selected curves with similar trends. The curves show the variation of the friction coefficient of OBM with increasing pressure at constant temperature of 50°C.
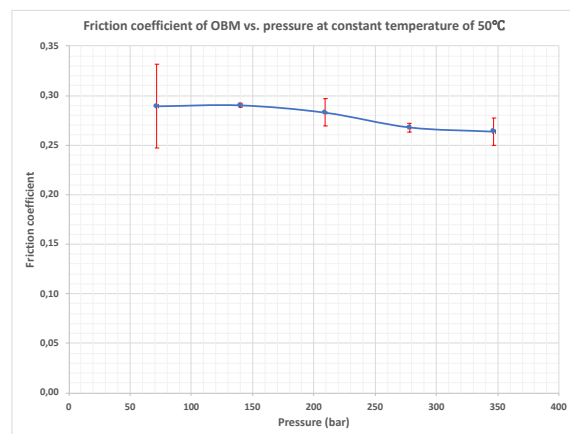
Fig. 4.14 A single trend showing the variation of friction coefficient of OBM with increasing pressure at constant temperature of 50°C. The red error bars show the standard deviation of the averaged data.

Table 4.6 Friction coefficient values of the OBM at constant temperatures of 25 and 50°C and different pressure steps.

OBM		
Pressure (bar)	**Friction coefficient at 25°C**	**Friction coefficient at 50°C**
69	0.47	0.29
138	0.47	0.29
207	0.54	0.28
276	0.65	0.27
345	0.90	0.26

As it can be observed in Fig. 4.11, the friction coefficient values of test 3 are consistently higher than those of tests 1 and 2. The two following reasons may have resulted in the significant increase of friction coefficient values in test 3.

- The existence of particles, particularly barite, in the OBM.
    - These particles may get stuck between the setup paddles and the slurry cup's wall and lead to an increase in the friction coefficient values.
- Sudden axial movements of the setup paddles.
    - As mentioned earlier, the lengths of the setup paddles are quite large. Thereby, the setup paddles can experience sudden axial movements during the experiments and lead to sudden increase in the friction coefficient values.

Nevertheless, it was decided to use the curve of test 3 together with the curves of tests 1 and 2 because they all showed an increasing trend of friction coefficient versus pressure. As it can be seen in Fig. 4.12, at constant temperature of 25℃, the friction coefficient of OBM increases with increasing pressure, on average by 90% between 0.47 at 69 bar and 0.90 at 345 bar. Instead, as it can be observed in Fig. 4.14, at constant temperature of 50℃, the friction coefficient of the OBM shows a very small decrease with increasing pressure. However, due to the spread of the measurements, one could also interpret this trend as approximately constant within the range of 0.26 and 0.29.

4.4.2 The effect of temperature on the friction coefficient

Fig. 4.15 illustrates the effect of temperature on the friction coefficient of the OBM. Also, Table 4.7 shows the corresponding numerical data and provides the percentage decrease in the friction coefficient values of the OBM as the temperature changes from 25 to 50℃ at each pressure step. As shown, the friction coefficient values of the OBM are systematically smaller during the experiments at constant temperature of 50℃ compared to the values at constant temperature of 25℃. As the temperature changes from 25 to 50℃, the friction coefficient decreases. Also, this decrease grows with increasing pressure (-38% at 69 bar up to -71% at 345 bar). This is the expected behavior, due to the decrease in the viscosity of the OBM with increasing temperature, which leads to lower friction coefficient values.
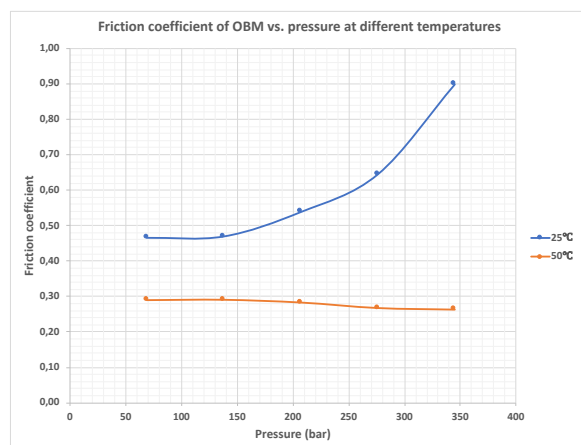
Fig. 4.15 Comparison of the friction coefficient values of OBM at temperatures of 25 and 50°C.

Table 4.7 Percentage decrease in friction coefficient of the OBM as the temperature changes from 25 to 50°C at each pressure step.

OBM			
Pressure (bar)	**Friction coefficient at 25°C**	**Friction coefficient at 50°C**	**% Decrease in friction coefficient**
69	0.47	0.29	-38
138	0.47	0.29	-38
207	0.54	0.28	-48
276	0.65	0.27	-58
345	0.90	0.26	-71

4.4.3 The effect of temperature on the viscosity of the OBM

As shown in Fig. 4.15, as the temperature changes from 25 to 50°C, there is a significant decrease in the friction coefficient values of the OBM. To investigate whether this significant decrease could be explained by a decrease of the viscosity of the base oil with increasing temperature, rheology tests were performed. These tests were done on the same OBM samples tested in the consistometer at temperatures of 25 and 50°C, respectively. The viscometer used for the rheology tests is shown in Fig. 4.16.

Fig. 4.16 Viscometer used for the rheology tests.

The rheology tests were performed right after the OBM was removed from the slurry cup of the consistometer after each series of five experiments at the defined temperatures. The OBM was then mixed using a mud mixer and poured into the viscometer's test cup. Fig. 4.17 illustrates a picture of the mud mixer.

Fig. 4.17 Mud mixer.

Fig. 4.18 shows the results of such tests, i.e. variation of the OBM's shear stress versus shear rate at temperatures of 25 and 50°C.
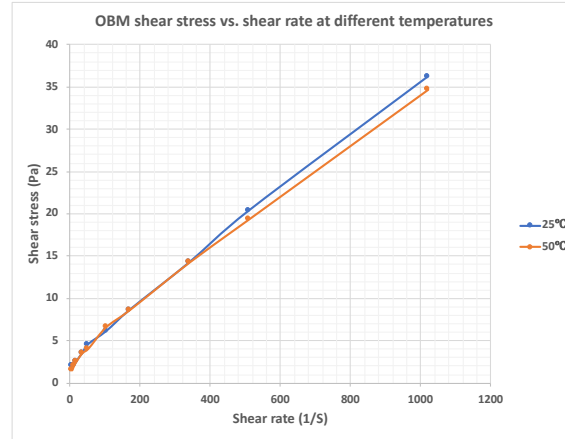
Fig. 4.18 The variation of the OBM's shear stress versus shear rate after performing each series of five experiments at temperatures of 25 and 50°C.

One can see that at temperature of 50°C the shear stress values of the OBM and, consequently, its viscosity, decrease by an average of -4% compared to the values at temperature of 25°C. So, one would be led to conclude that these measurements indicate that a decrease of viscosity of the OBM with temperature cannot be the main cause of the significant decrease of the friction coefficient shown in Fig. 4.15. However, one must consider that they may have been affected by an important methodological artefact: in fact, it took approximately 10 minutes to prepare the mud for the rheology tests after the measurements in the consistometer and during that time the fluid was exposed to room temperature. Also, the viscometer itself performed the measurements at room temperature. Consequently, it may be assumed that the mud was colder during the rheology tests than when it was tested in the consistometer, and that this cooling effect was larger for the samples originally at 50°C. Therefore, the actual temperature of the samples originally at different temperatures may have not been that different when they were tested in the viscometer and consequently, also their measured viscosity.

4.5 Water-based drilling fluid (WBM)

The WBM used for the experiments was also made at the drilling fluid laboratory at the University of Stavanger. Table 4.8 shows its composition.

Table 4.8 The composition of the WBM

Materials	Quantity	Unit
Deionized water	350	ml
DUO-TEC NS	1.5	g
POLYPAC ELV	6	g
GLYDRIL MC	15	ml
5% NaOH solution	10	ml

4.5.1 The effect of pressure on the friction coefficient

Five experiments were performed on the WBM at constant temperature of 25°C while the pressure increased up to 345 bar. Fig. 4.19 shows the three selected curves of the friction coefficient of the WBM versus pressure which had similar trends. Also, Fig. 4.20 is a plot of the average trend together with the standard deviations per each pressure value. Similarly, Fig. 4.21 and Fig. 4.22 show the same data for the measurements at 50°C. Finally, Table 4.9 reports the corresponding numerical values.
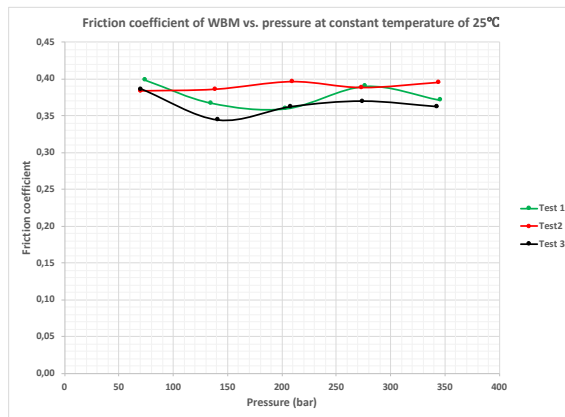
Fig. 4.19 Three selected curves with similar trends. The curves show the variation of the friction coefficient of WBM with increasing pressure at constant temperature of 25°C.
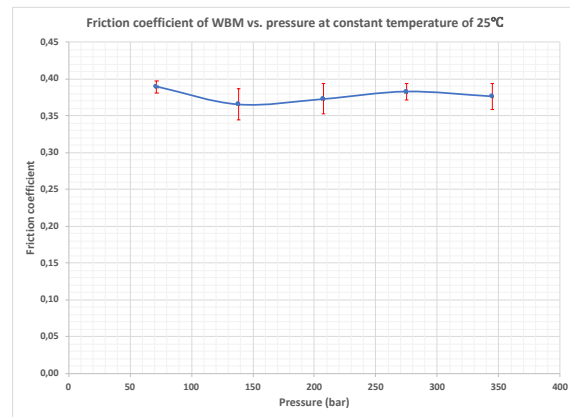
Fig. 4.20 A single trend showing the variation of friction coefficient of WBM with increasing pressure at constant temperature of 25°C. The red error bars show the standard deviation of the averaged data.
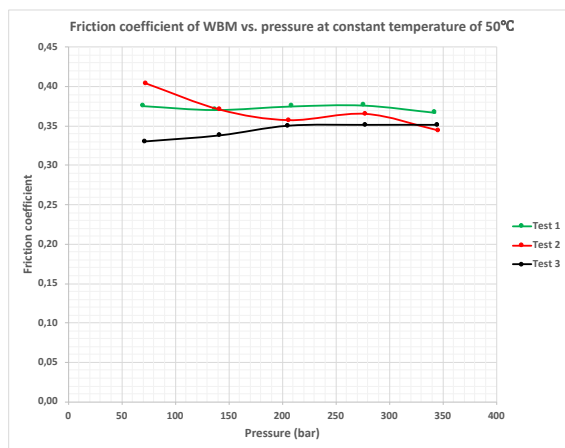
Fig. 4.21 Three selected curves with similar trends. The curves show the variation of the friction coefficient of WBM with increasing pressure at constant temperature of 50°C.
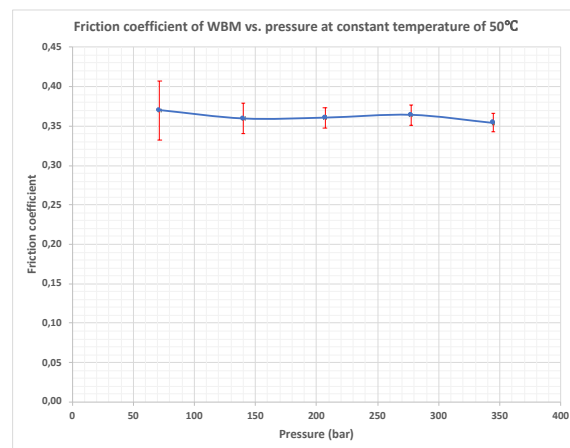
Fig. 4.22 A single trend showing the variation of friction coefficient of WBM with increasing pressure at constant temperature of 50°C. The red error bars show the standard deviation of the averaged data.

Table 4.9 Friction coefficient values of WBM at constant temperatures of 25 and 50°C and different pressure steps.

WBM		
Pressure (bar)	**Friction coefficient at 25°C**	**Friction coefficient at 50°C**
69	0.39	0.37
138	0.37	0.36
207	0.37	0.36
276	0.38	0.36
345	0.38	0.35

As it can be observed in Fig. 4.20 and Fig. 4.22, at both temperatures the friction coefficient of the WBM has a constant trend with increasing pressure. Moreover, both sets of experiments showed quite consistent results, with a very low standard deviation which exceeded 1% in only

one case (at 69 bar at 50°C, Fig. 4.22): this indicates that, in spite of the challenges that the designed setup encountered as explained in section 3.3, the experimental conditions during the tests at the same temperature were essentially the same.

Also, as it can be observed from Table 4.9, at constant temperature of 25°C, the friction coefficient values of the WBM are almost constant and close to an average value of 0.38. Similarly, at constant temperature of 50°C, the friction coefficient values of the WBM seem to be approximately constant and close to an average value of 0.36. Therefore, increasing pressure does not seem to have a significant effect on the friction coefficient of the WBM.

4.5.2 The effect of temperature on the friction coefficient

Fig. 4.23 indicates the effect of temperature on the friction coefficient of WBM. Essentially, the measured values at both temperatures are very similar at any pressure, i.e., between 0.37 and 0.39 at 25°C and between 0.35 and 0.37 at 50°C. All the values at 50°C are lower than those at 25°C (on average -4%), likely due to a small effect of decrease in the viscosity of the WBM. Table 4.10 provides the percentage decrease in the friction coefficient values of the WBM as the temperature changes from 25 to 50°C at each pressure step.
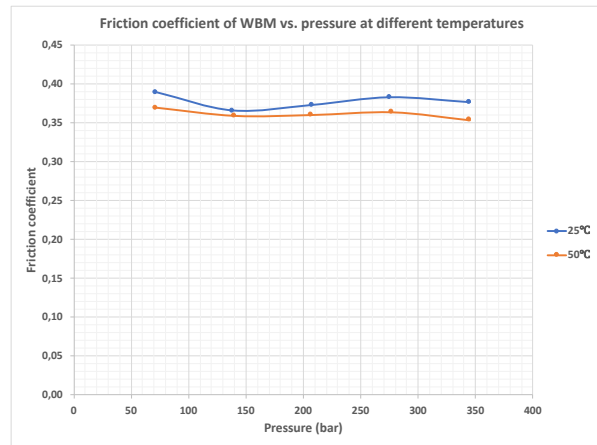
Fig. 4.23 Comparison of the friction coefficient values of WBM at constant temperatures of 25 and 50°C.

Table 4.10 Percentage decrease in friction coefficient of the WBM as the temperature changes from 25 to 50°C at each pressure step.

WBM			
Pressure (bar)	**Friction coefficient at 25°C**	**Friction coefficient at 50°C**	**% Decrease in friction coefficient**
69	0.39	0.37	-5
138	0.37	0.36	-2
207	0.37	0.36	-3
276	0.38	0.36	-5
345	0.38	0.35	-6

4.5.3 The effect of temperature on the viscosity of the WBM

Similar to what was done for the OBM, also the WBM samples were tested in a viscometer to investigate whether a decrease of their viscosity with temperature can explain the decrease of the friction coefficient, as shown in Fig. 4.23. The same procedure used for the OBM samples was applied to the WBM samples (see section 4.4.3) and the results are shown in Fig. 4.24.
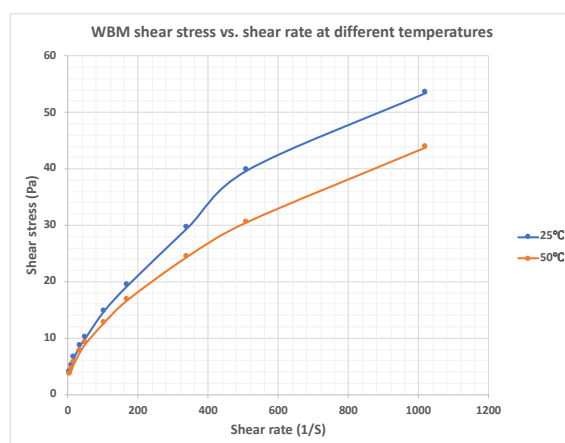
Fig. 4.24 The variation of the WBM's shear stress versus shear rate after performing each series of five experiments at temperatures of 25 and 50°C.

The rheology tests of WBM were also affected by the same methodological artefact as the OBM samples (i.e. the samples were cooling down from their original temperature before and during the measurements in the viscometer). However, the measured shear stress values of the WBM samples originally at 50°C decreased by an average of -15% compared to the samples originally at temperature of 25°C. In this case, therefore, it was possible to verify, at least in a semi-quantitative way, that the decrease of the friction coefficient with increased temperature shown in Fig. 4.23 may be explained by the decrease of viscosity of the WBM.

4.6 Comparison of the results among the four fluids

The same datasets shown and discussed in the previous sections can be used to compare the behavior of the four different fluids at the same experimental conditions and to investigate the differences among them. Fig. 4.25 compares the measurements made at 25℃, while Fig. 4.26 shows those at 50℃.
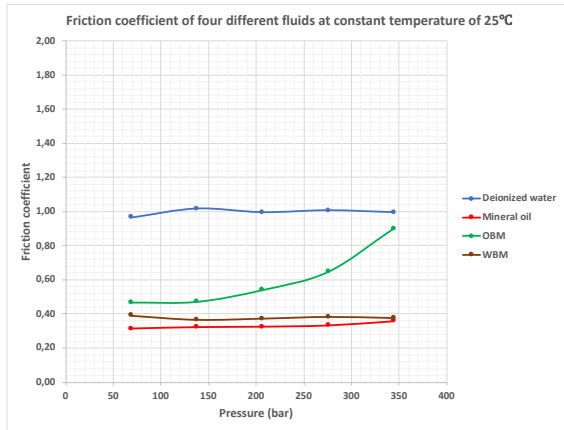
| **Fig. 4.25** Comparison of the friction coefficients of four different fluids at constant temperature of 25℃. | **Fig. 4.26** Comparison of the friction coefficients of four different fluids at constant temperature of 50℃. |
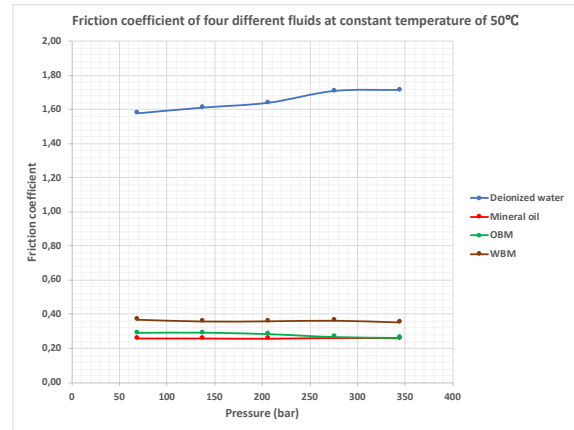
From the experimental data shown in Fig. 4.25 and Fig. 4.26, one can observe that:

- The deionized water is by far the fluid with the largest friction coefficient at both temperatures.

- If one excludes the trend of the OBM at 25℃ (the green curve in Fig. 4.25), the effect of increasing pressure on the friction coefficient is almost negligible for all the fluids or, at most, very small as in the case of the deionized water at 50℃ (increase by +9%, the blue curve in Fig. 4.26).

- The peculiar trend of the OBM at 25℃ with respect to all the other measurements suggests that likely these results were affected by experimental artefacts (section 3.3) and should not be taken as very reliable. In this respect, one should note that Fig. 4.11, in which the individual repeated measurements are plotted, shows that for two tests out of three, the measured values of the friction coefficient were almost constant at low pressures and similar to the other fluids (about 0.40). This is a further indication that very likely experimental artefacts affected both all the measurements of test 3 and those of tests 1 and 2 at high pressures.

- The mineral oil Calpar (100R) provides the lowest friction coefficient at any experimental condition considered in this study: for instance, at the pressure of 207 bar its friction coefficient with respect to the WBM is 14% lower at 25℃ and 28% lower at 50℃; the same comparison with the OBM can be done at the pressure of 207 bar only at 50℃, and the result is that it is 7% lower.

- The OBM provides a lower friction coefficient with respect to the WBM (-22%), at least at 50℃, i.e. in the only condition where the results for the OBM are reliable.

5 CONCLUSION

Considering the results presented and discussed in section 4, the following conclusions can be drawn:

- With the exclusion of deionized water at 50℃ and the OBM at 25℃, the effect of increasing pressure on the friction coefficient of the other fluids seems to be negligible. In the case of deionized water at 50℃, the friction coefficient values increased by +9% with increasing pressure. However, the results of the experiments with the OBM at 25℃ might not be considered as very reliable due to the experimental challenges.

- On the other hand, the temperature showed a decreasing effect on the friction coefficient values of all the fluids except deionized water. The decrease of the friction coefficient values of the fluids with increasing temperature could be justified by the fact that the viscosity of the fluids decreases with increasing temperature and consequently, their lubricity effect increases. However, in the case of deionized water, the results showed that the friction coefficient increases with temperature at all the pressure steps. This could be due to the experimental challenges.

- By comparing the friction coefficient values of the four fluids at temperatures of 25 and 50℃ and increasing pressure up to 345 bar, it can be concluded that:

  o The mineral oil has the lowest friction coefficient values compared to the other fluids at both temperatures while deionized water has the highest values.

  o At the temperature of 50℃, the OBM shows lower friction coefficient values (about -22%) compared to the WBM. On the other hand, at the temperature of 25℃ the OBM has higher friction coefficient values compared to those of WBM. In this case, the comparison could be mostly qualitative, due to the setup challenges, which affected the measurements at 25℃ of the OBM.

6 SUGGESTED IMPROVEMENTS AND ACTIVITIES

In this project, the challenges with the specially designed setup were investigated (section 3.3). Also, possible changes that should be implemented in the setup design for future experiments were suggested (section 3.4). In this section, three considerations with respect to the test fluids are also listed that should be taken into account for increasing the reliability of the results of the future experiments.

1. The particles included in the OBM and the WBM might get stuck between the setup paddles and the slurry cup's inside wall. This will result in unexpected high friction coefficient values. To avoid this issue in the future experiments, it is thus recommended to use drilling fluids with smaller particles (e.g. with micronized barite).

2. The drilling fluids must be properly mixed prior to the experiments (approximately 5 to 10 minutes). During the mixing procedure, small air bubbles will form inside the drilling fluids. Thereby, to remove the air bubbles, it is recommended to use a plastic hammer and slowly tap the cup which holds the drilling fluid. Once the air bubbles are properly removed, the drilling fluids are ready to be used for the experiments. Removal of the air bubbles prior to the experiments is essential as their presence can affect the friction coefficient values of the drilling fluids.

3. Based on the results of the experiments in this project, it was concluded that temperature can affect the viscosity of all the test fluids and consequently, their lubricity effect and friction coefficient values. To analyze this effect experimentally, it is recommended to measure the viscosity of all the test fluids at the desired test temperatures.

7 REFERENCES

Aarrestad, T.V., 1994. Torque and drag-two factors in extended-reach drilling. Journal of Petroleum Technology, 46(09), 800-803. https://doi.org/10.2118/27491-PA.

Amanullah, M. 2016. Coefficient of Friction Reducing Efficiency of ARC Eco-Lube. Presented at the IADC/SPE Asia Pacific Drilling Technology Conference, Singapore. 22-24 August. SPE-180504-MS. https://doi.org/10.2118/180504-MS.

API. 2013. Recommended practice for testing well cements.

Barraez, R., Noland, J., Matheus, D., Spence, Z. 2014. Comprehensive Analysis of Metal-to-Metal Lubricants in Oil Shale Plays. *Proc.*, SPE/ICoTA Coiled Tubing and Well Intervention Conference and Exhibition, The Woodlands, Texas, USA, 25-26 March. SPE-168280-MS. https://doi.org/10.2118/168280-MS.

Beal, C., 1946. The Viscosity of Air, Water, Natural Gas, Crude Oil and Its Associated Gases at Oil Field Temperatures and Pressures. SPE-946094-G, 165(01), 94-115. https://doi.org/10.2118/946094-G.

Bhushan, B., 2013. Principles and Applications of Tribology. John Wiley & Sons.

Bourgoyne Jr, A.T., Millheim, K.K., Chenevert, M.E., Young Jr, F.S., 1986. Applied drilling engineering.

Bowden, F.P., Tabor, D., 1964. The friction and lubrication of solids part II. Clarendon Press.

Breeden, D., Dougan, C., Shank, D., Summers, S., 2011. Haynesville performance review: Unique clay-free water-based polymer drilling fluid system for application-specific unconventional shale production intervals, AADE-11-NTCE-39, Houston, TX.

Bridgman, P.W., 1949. The Physics Of High Pressure. G. Bell And Sons Ltd., London.

Caenn, R., Darley, H.C.H., Gray, G.R., 2016. Composition and Properties of Drilling and Completion Fluids, 7. Elsevier Science.

Craig, S. 2003. A multi-well review of coiled tubing force matching. *Proc.*, SPE/ICoTA Coiled Tubing Conference and Exhibition, Houston, Texas, 8-9 April. SPE-81715-MS. https://doi.org/10.2118/81715-MS.

Dowson, D., 1998. History of tribology Professional Engineering Publishing Limited.

Dzialowski, A., Hale, A., Mahajan, S. 1993. Lubricity and Wear of Shale: Effects of Drilling Fluids and Mechanical Parameters. Presented at the SPE/IADC Drilling Conference, Amsterdam, Netherlands. 22-25 February. SPE-25730-MS. https://doi.org/10.2118/25730-MS.

Foxenberg, W.E., Ali, S.A., Long, T.P., Vian, J. 2008. Field experience shows that new lubricant reduces friction and improves formation compatibility and environmental impact. *Proc.*, SPE International Symposium and Exhibition on Formation Damage Control, Lafayette, Louisiana, USA, 13-15 February. SPE-112483-MS. https://doi.org/10.2118/112483-MS.

Gee, R., Hanley, C., Hussain, R., Canuel, L., Martinez, J. 2015. Axial Oscillation Tools vs. Lateral Vibration Tools for Friction Reduction–What's the Best Way to Shake the Pipe? *Proc.*, SPE/IADC Drilling Conference and Exhibition, London, England, UK, March 17-19 SPE-173024-MS. https://doi.org/10.2118/173024-MS.

Growcock, F.B., Frederick, T.P., Reece, A.R., Green, G.W., Ruffin, M.D. 1999. Novel Lubricants for Water-Based Drilling Fluids. Presented at the SPE International Symposium on Oilfield Chemistry, Houston, Texas. 16-19 February. SPE-50710-MS. https://doi.org/10.2118/50710-MS.

Holand, J., Kvamme, S.A., Omland, T.H., Saasen, A., Taugbol, K., Jamth, J. 2007. Lubricant enabled completion of ERD well. Presented at the SPE/IADC Drilling Conference, Amsterdam, The Netherlands. February 20-22. SPE-105730-MS. https://doi.org/10.2118/105730-MS.

Holder, B.J., 1982. Drilling Fluids for Highly Deviated Wells in North Sea Petroleum Drilling. Journal of Petroleum Technology, 34(04), 703-712. https://doi.org/10.2118/10860-PA.

Ismail, A.R., Rashid, M.S.A., Ismail, N.J., Sulaiman, W.R.W., Jaafar, M.Z., 2015. Improved Coefficient of Friction Using Different Types of Lubricants in Drilling Operation. 1125, 210-214. https://doi.org/10.4028/www.scientific.net/AMR.1125.210.

Johancsik, C., Friesen, D., Dawson, R., 1984. Torque and drag in directional wells-prediction and measurement. Journal of Petroleum Technology, 36(06), 987-992. https://doi.org/10.2118/11380-PA.

Kaarstad, E., Aadnoy, B.S., Fjelde, T. 2009. A study of temperature dependent friction in wellbore fluids. *Proc.*, SPE/IADC Drilling Conference and Exhibition, Amsterdam, The Netherlands, March 17-19 SPE/IADC 119768. https://doi.org/10.2118/119768-MS.

Ke, M., Foxenberg, W.E. 2010. Lubricity of brine completion and workover fluids. *Proc.*, SPE/ICoTA Coiled Tubing and Well Intervention Conference and Exhibition, The Woodlands, Texas, USA, March 23-34. SPE-130679-MS. https://doi.org/10.2118/130679-MS.

Knežević, D., Savić, V., 2006. Mathematical modeling of changing of dynamic viscosity, as a function of temperature and pressure, of mineral oils for hydraulic systems. Facta Universitatis. Series. Mechanical Engineering (Serbia), 4, 27-34.

Livescu, S., Craig, S. 2014. Increasing Lubricity of Downhole Fluids for Coiled Tubing Operations. Presented at the SPE/ICoTA Coiled Tubing and Well Intervention Conference and Exhibition, The Woodlands, Texas, USA. March 25-26. SPE-168298-PA. https://doi.org/10.2118/168298-PA.

Livescu, S., Craig, S., 2017. A critical review of the coiled tubing friction-reducing technologies in extended-reach wells. Part 1: Lubricants. Journal of Petroleum Science and Engineering, 157, 747-759. https://doi.org/10.1016/j.petrol.2017.07.072.

Livescu, S., Craig, S.H., Watkins, T. 2014. Challenging the Industry's Understanding of the Mechanical Friction Reduction for Coiled Tubing Operations. *Proc.*, SPE Annual Technical Conference and Exhibition, Amsterdam, The Netherlands, October 27-29 SPE-170635-MS. https://doi.org/10.2118/170635-MS.

Maidla, E.E., Wojtanowicz, A., 1990. Laboratory study of borehole friction factor with a dynamic-filtration apparatus. 5(03), 247-255. https://doi.org/10.2118/18558-PA.

McCormick, J.E., Evans, C.D., Le, J., Chiu, T. 2011. The practice and evolution of torque and drag reduction: theory and field results. *Proc.*, International Petroleum Technology Conference. https://doi.org/10.2523/IPTC-14863-MS.

Mirhajmohammadabadi, S.A., Fazaelizadeh, M., Kaarstad, E., Aadnoy, B.S. 2010. New Aspects of Torque-and-Drag Modeling in Extended-Reach Wells. *Proc.*, SPE Annual Technical Conference and Exhibition, Florence, Italy, 19-22 September. SPE-135719-MS. https://doi.org/10.2118/135719-MS.

Mitchell, R.F., Samuel, R. 2007. How Good is the Torque-Drag Model? *Proc.*, SPE/IADC Drilling Conference, Amsterdam, The Netherlands, February 20-22. SPE-105068-MS. 62-71. https://doi.org/10.2118/105068-MS.

OFITE, 2010. MATERIAL SAFETY DATA SHEET. http://www.ofite.com/doc/120-001-005.pdf (accessed 25 March 2019).

OFITE, 2019a. Lubricity Tester. http://www.ofite.com/products/drilling-fluids/product/2229-lubricity-tester (accessed 04 February 2019).

OFITE, 2019b. Model 2040 Automated HTHP Cement Consistometer, 40 KSI, 600°F. http://www.ofite.com/products/cement-testing/thickening-time/product/85-model-2040-automated-hthp-consistometer (accessed 09 March 2019).

OFITE, 2019c. Thermocup with Removable Stainless Steel Cup. http://www.ofite.com/products/drilling-fluids/product/2310-thermocup-with-removable-stainless-steel-cup (accessed 09 April 2019).

Patel, A., Zhang, H.J., Ke, M., Panamarathupalayam, B. 2013. Lubricants and drag reducers for oilfield applications-chemistry, performance, and environmental impact. *Proc.*, SPE International Symposium on Oilfield Chemistry, The Woodlands, Texas, USA. SPE-164049-MS. https://doi.org/10.2118/164049-MS.

Persson, B.N.J., 2000. Sliding friction : physical principles and applications. Nanoscience and technology, 2nd ed. Springer, Berlin.

Quigley, M.C. 1989. Advanced Technology for Laboratory Measurements of Drilling Fluid Friction Coefficient. Presented at the SPE Annual Technical Conference and Exhibition, San Antonio, Texas. 8-11 October. SPE-19537-MS. https://doi.org/10.2118/19537-MS.

Rabinowicz, E., 1995. Friction and Wear of Materials. Inc., New York, 2nd edition.

Redburn, M., Dearing, H., Growcock, F. 2013. Field lubricity measurements corrilate with improved performance of novel water-based drilling fluid. *Proc.*, Offshore Mediterranean Conference and Exhibition, Ravenna, Italy, March 20-22. OMC-2013-159.

Samuel, G.R., 2007. Downhole drilling tools : theory and practice for engineers and students. Gulf Pub., Houston, TX.

Samuel, R. 2010. Friction factors: What are they for torque, drag, vibration, bottom hole assembly and transient surge/swab analyses? Presented at the IADC/SPE Drilling Conference and Exhibition, New Orleans, Louisiana, USA. https://doi.org/10.2118/128059-MS.

Schamp, J.H., Estes, B.L., Keller, S.R. 2006. Torque Reduction Techniques in ERD Wells. Presented at the IADC/SPE Drilling Conference, Miami, Florida, USA. 21-23 February. SPE-98969-MS. https://doi.org/10.2118/98969-MS.

Sheppard, M., Wick, C., Burgess, T., 1987. Designing well paths to reduce drag and torque. SPE Drilling Engineering, 2(04), 344-350. https://doi.org/10.2118/15463-PA.

Skalle, P., 2011. Drilling fluid engineering. Bookboon.

Sönmez, A., Kök, M.V., Özel, R., 2013. Performance analysis of drilling fluid liquid lubricants. Journal of Petroleum Science and Engineering, 108, 64-73. https://doi.org/10.1016/j.petrol.2013.06.002.

Taghipour, A., Ytrehus, J.D., Lund, B., Saasen, A. 2014. The effect of different drilling fluids on borehole mechanical friction. *Proc.*, ASME 2014 33rd International Conference on Ocean, Offshore and Arctic Engineering. OMAE2014-23959. V005T11A016-V005T11A016. https://doi.org/10.1115/OMAE2014-23959.

Taghipour, A., Ytrehus, J.D., Lund, B., Skalle, P., Lund, M., Prakash, B., 2015. Friction and wear characteristics of steel on rock under water and oil based lubricated sliding conditions. Tribology - Materials, Surfaces & Interfaces, 9(2), 85-91. https://doi.org/10.1179/1751584X15Y.0000000004.

Walker, M.W. 2012. Pushing the Extended-Reach Envelope at Sakhalin: An Operator. Presented at the IADC/SPE Drilling Conference and Exhibition, San Diego, California, USA. 6-8 March. SPE-151046-MS. https://doi.org/10.2118/151046-MS.

Wang, P., Ni, H., Wang, R., 2018. A novel vibration drilling tool used for reducing friction and improve the penetration rate of petroleum drilling. Journal of Petroleum Science Engineering, 165, 436-443. https://doi.org/10.1016/j.petrol.2018.02.053.

Wonham, J., 1967. Effect of Pressure on the Viscosity of Water. Nature, 215(5105), 1053-1054. https://doi.org/10.1038/2151053a0.

Ytrehus, J.D., Taghipour, A., Golchin, A., Saasen, A., Prakash, B., 2017. The Effect of Different Drilling Fluids on Mechanical Friction. Journal of Energy Resources Technology, 139(3). https://doi.org/10.1115/1.4035951.

Ytrehus, J.D., Taghipour, A., Lund, B., Gyland, K.R., Saasen, A. 2016. Experimental Investigation of Mechanical Friction and Hydraulics for Liner Drilling and Liner Running. *Proc.*, ASME 2016 35th International Conference on Ocean, Offshore and Arctic Engineering, Busan, South Korea, June 19-24. OMAE2016-54049. https://doi.org/10.1115/OMAE2016-54049.

8 APPENDIX A

8.1 The plots generated by the UCS tester

As mention in section 3.5.1, five experiments were performed on the setup's spring for the purpose of finding the spring constant as a function of temperature. The UCS tester then created five plots of applied load versus spring deformation for each temperature. By using the trend line function in Microsoft Excel, the slopes of the plots which showed the spring constant at each temperature were computed. Fig. 8.1 to Fig. 8.5 illustrate these plots.
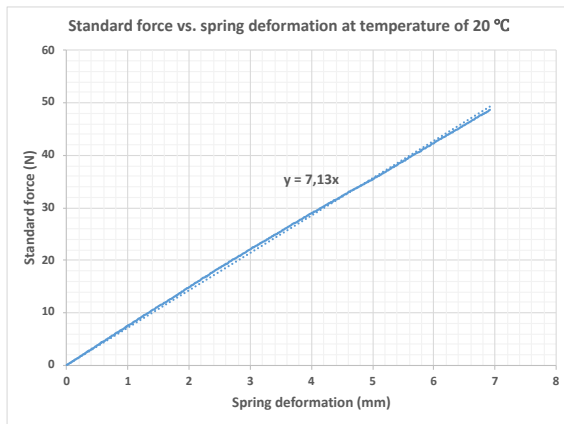

Fig. 8.1 Standard force versus spring deformation at temperature of 20℃. The slope of the line shows the spring constant at this temperature.
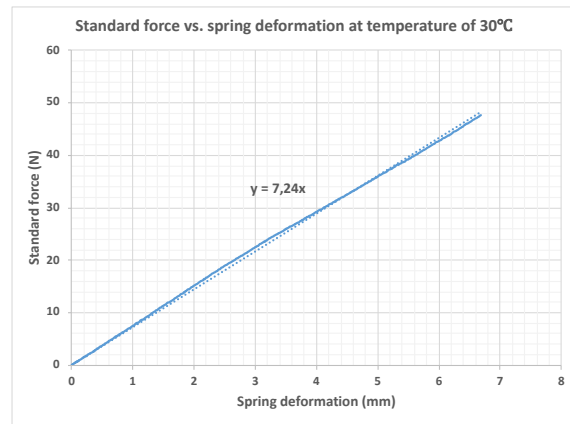

Fig. 8.2 Standard force versus spring deformation at temperature of 30℃. The slope of the line shows the spring constant at this temperature.

Fig. 8.3 Standard force versus spring deformation at temperature of 40℃. The slope of the line shows the spring constant at this temperature.

Fig. 8.4 Standard force versus spring deformation at temperature of 50℃. The slope of the line shows the spring constant at this temperature.

Fig. 8.5 Standard force versus spring deformation at temperature of 60°C. The slope of the line shows the spring constant at this temperature.
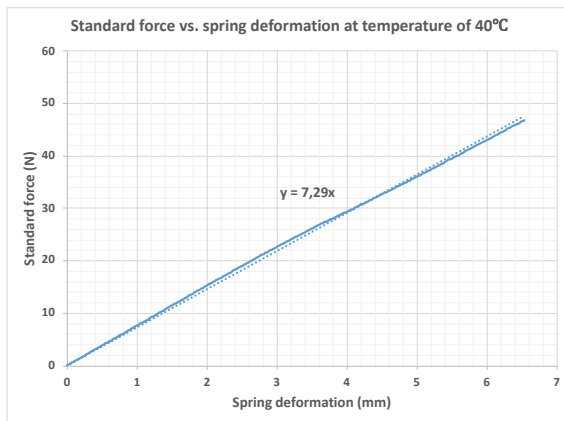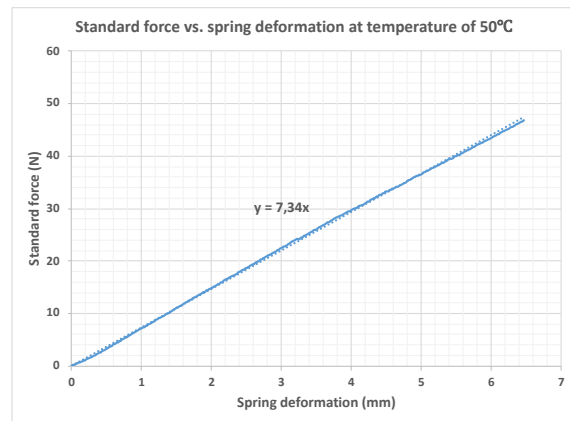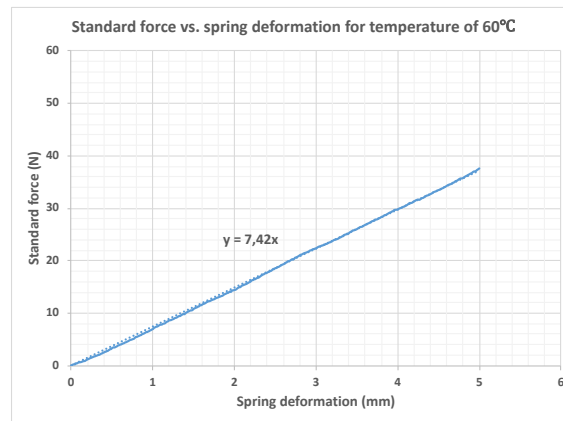
9 APPENDIX B

9.1 The results of the primary experiments with the newly designed setup

Prior to the work of this thesis, a series of experiments were perform using the newly designed setup. The results of these experiments were included in a conference paper which was approved to be published and presented in the international conference on Ocean, Offshore and Arctic Engineering (OMAE 2019). The first page of this conference paper is provided in this section.

OMAE2019-96594

MECHANICAL FRICTION IN WELL CONSTRUCTION AND LABORATORY TESTING OF FRICTION COEFFICIENTS

Parisa Ghaedi
University of Stavanger
Stavanger, Norway

Mahmoud Khalifeh
University of Stavanger
Stavanger, Norway

Arild Saasen
University of Stavanger
Stavanger, Norway

Helge Hodne
University of Stavanger
Stavanger, Norway

Tor H. Omland
Equinor
Stavanger, Norway

Farzad Shoghl
Equinor
Stavanger, Norway

ABSTRACT

A new device for measuring the lubricity of drilling fluids for controlling the mechanical friction is developed. This is able to measure mechanical friction at temperatures between room temperature and 200°C and at pressures in the range of atmospheric to 20 000 psi. The effects of lubricants on mechanical friction is outlined. Different types of available test instruments are reviewed. These instruments include both commercial equipment and special designed equipment. In addition, the effect of pressure and temperature as well as their combined effect on the friction coefficient of deionized water, mineral oil and oil-based mud (OBM) have been investigated as initial test of the developed instrument. Our initial results show that friction coefficient increases with pressure increase for the mineral oil and OBM, at 25°C. However, when deionized water was used as lubricant, the friction coefficient decreased when pressure was increased.

INTRODUCTION

Generally, friction is a force which acts against the direction of motion of two objects which are moving relative to each other. Friction belongs to the science of tribology. Tribology itself originates from the Greek word tribos which means rubbing and rubbing is the phenomenon which occurs when two surfaces move and slide relative to each other. The pioneers of the science of tribology, Amonton and Coulomb came up with three laws of friction [1]. The first of which states that the friction force is directly proportional to the load which is applied to the objects in motion. The second which states that the friction force does not depend on the apparent area of contact. This means that the interlocking asperities inside the two objects in contact should overcome the friction force in order for the motion to initiate and thus the area of contact between two objects does not affect the friction force. The third friction law states that the kinetic friction does not depend on the velocity of the sliding objects. Kinetic friction force is a force which is acting opposite to the direction of the motion of the object and it makes the movement more difficult for each object moving relative to another one. So, no matter how fast the object is moving, the friction force will always exist.

The friction coefficient is defined as the ratio between the friction force of the two objects in contact and the normal force applied to them. The friction coefficient can be calculated using Eq. 1.

$$\mu_i = \frac{F_f}{N} \tag{1}$$

where μ_i is the static or kinetic coefficient of friction, F_f is the force of friction and N is the normal force.

The friction coefficient depends on several parameters such as temperature, pressure, surface roughness, embedded fluid viscosity, applied load, humidity, etc. [1]. To be able to predict the necessary force to be able to run in casings, liners or completion strings, the friction coefficient in the different sections of a wellbore must be estimated properly.

In a wellbore, mechanical friction must be overcome in several situations. For example, the friction between drillpipe or tubing and casing, which can be an example of steel on steel mechanical friction. Also, the friction between drillpipe or drill bit and formation is an example of steel on rock mechanical friction. Understanding and handling the mechanical friction is of concern in different operations during the lifetime of a well as it can lead to various challenges. Among many challenges caused by mechanical friction one can refer to limitation of running and tripping speed of drill strings and liners [2], excessive torque and drag which by itself can result in stuck pipe, pipe buckling or even complete loss of the well [3]. In addition,